Stellar rotation in the Hyades and Praesepe: gyrochronology and braking time-scale

P. Delorme, A. Collier Cameron, L. Hebb, J. Rostron, T. Lister, A. Norton, D. Pollacco, R. West

Monthly Notices
of the
ROYAL ASTRONOMICAL SOCIETY

Mon. Not. R. Astron. Soc. **413,** 2218–2234 (2011) doi:10.1111/j.1365-2966.2011.18299.x

Stellar rotation in the Hyades and Praesepe: gyrochronology and braking time-scale

P. Delorme,[1⋆] A. Collier Cameron,[1] L. Hebb,[2] J. Rostron,[1] T. A. Lister,[3] A. J. Norton,[4] D. Pollacco[5] and R. G. West[6]

[1]*SUPA, School of Physics and Astronomy, University of St Andrews, North Haugh, St Andrews, Fife KY16 9SS*
[2]*Department of Physics and Astronomy, Vanderbilt University, 6301 Stevenson Center, Nashville, TN 37235, USA*
[3]*Las Cumbres Observatory, 6740 Cortona Dr. Suite 102, Santa Barbara, CA 93117, USA*
[4]*Department of Physics and Astronomy, The Open University, Milton Keynes MK7 6AA*
[5]*Astrophysics Research Centre, School of Mathematics & Physics, Queen's University, University Road, Belfast BT7 1NN*
[6]*Department of Physics and Astronomy, University of Leicester, Leicester LE1 7RH*

Accepted 2011 January 4. Received 2011 January 4; in original form 2010 July 22

ABSTRACT

We present the results of photometric surveys for stellar rotation in the Hyades and in Praesepe, using data obtained as part of the SuperWASP exoplanetary transit-search programme. We determined accurate rotation periods for more than 120 sources whose cluster membership was confirmed by common proper motion and colour–magnitude fits to the clusters' isochrones. This allowed us to determine the effect of magnetic braking on a wide range of spectral types for expected ages of ∼600 Myr for the Hyades and Praesepe. Both clusters show a tight and nearly linear relation between $J - K_s$ colour and rotation period in the F, G and K spectral range. This confirms that loss of angular momentum was significant enough that stars with strongly different initial rotation rates have converged to the same rotation period for a given mass, by the ages of Hyades and Praesepe. In the case of the Hyades, our colour–period sequence extends well into the M dwarf regime and shows a steep increase in the scatter of the colour–period relation, with identification of numerous rapid rotators from $\sim 0.5\,M_\odot$ down to the lowest masses probed by our survey ($\sim 0.25\,M_\odot$). This provides crucial constraints on the rotational braking time-scales and further clears the way to use gyrochronology as an accurate age measurement tool for main-sequence stars.

Key words: techniques: photometric – surveys – stars: rotation – open clusters and associations: individual: Hyades, Praesepe.

1 INTRODUCTION

The coeval populations of stars in galactic open clusters provide the best laboratories we have for testing theories of stellar evolution. The understanding we have gained from modelling their colour–magnitude diagrams allows us to determine the ages of open-cluster populations with far greater confidence than is possible for any individual field star. Following the establishment of an age sequence for open clusters, studies of stellar rotation by Kraft (1967), Skumanich (1972) and others revealed that the rotation rates of stars in open clusters decline with cluster age. The power-law spin-down with age $\Omega \propto t^{-1/2}$ is consistent with expectations from idealized models of angular momentum loss via the stellar equivalent of the hot, magnetically channelled solar wind (Weber & Davis 1967).

⋆E-mail: pd10@st-andrews.ac.uk

Photometric studies of rapid rotators in young open clusters flourished in the late 1980s, but precise measures of the spin periods among the slower rotators and in older clusters remained elusive. Radick et al. (1987) found that main sequence F, G and K in the Hyades show a far tighter period–colour relation than is found in the younger populations of the α Persei and Pleiades clusters. Models of spin-up and spin-down in the pre- and post-zero-age main sequence (ZAMS; e.g. Collier Cameron & Jianke 1994; Collier Cameron, Campbell & Quaintrell 1995; Bouvier, Forestini & Allain 1997) provided further confirmation that power-law spin-down should cause the spin rates of otherwise identical stars with different rotational histories to converge within a few hundred Myr of the ZAMS. These models employed the Weber–Davis formulation modified to take into account the dependance of the magnetic flux in the wind on rotation rate for the most rapidly spinning stars. As Barnes (2003) pointed out, this suggests a single-valued period–age relation for stars of a given mass older than the threshold age at which convergence occurs. Barnes (2007) provided the

first attempts at calibrating stellar spin-down as a clock, using asteroseismology and open clusters as primary age calibrators, and Mamajek & Hillenbrand (2008) proposed a modified age–rotation calibration.

The study of stellar rotation in open clusters has undergone something of a renaissance in the last few years, largely as a by-product of wide-field searches for transiting exoplanets in open clusters and in the field. The wide fields of view, superb photometric precision and long durations of these surveys are perfectly suited to determining the rotation distributions of young and intermediate-age open clusters with unprecedented completeness. Many such studies focusing on cluster of various ages are cited in the recent review by Irwin & Bouvier (2009). Since then, further studies of Coma Berenices (Collier Cameron et al. 2009), NGC 2301 (Sukhbold & Howell 2009), M34 (James et al. 2010), M35 (Meibom, Mathieu & Stassun 2009) and the Pleiades (Hartman et al. 2010) have been published.

As two of the closest (respectively 46 and 180 pc; van Leeuwen 2009) rich, intermediate-age open clusters to the Earth, the Hyades and Praesepe provide a vital calibration points for many types of stellar evolution study. Photometry, however, presents a severe challenge, owing to the wide angular extent of both clusters. Fortuitously, they both fall within the range of declinations surveyed by the northern camera array of the Wide-Angle Search for Planets (SuperWASP). Here we present studies of the distribution of rotation periods as a function of colour in both clusters, derived from SuperWASP photometry. For the first time, we extend the Hyades period–colour relation from the F, G and K stars studied by Radick et al., down to the late-K and M-dwarf population in which the magnetic braking process has not yet led to convergence.

After presenting in Section 2 the SuperWASP data we used for this study, we explain in Section 3 how we obtained the rotational periods of 70 stars in the Hyades cluster. Section 4 focuses on the determination of the period–colour relation in the Hyades and in Section 5 we extend this work and apply it to the Praesepe cluster. Section 6 is dedicated to the comparison between the Hyades, Praesepe and Coma, with the determination of their relative ages. We use this age information, together with the rotational data to put strong constraints on the magnetic braking time-scales. The last section deals with the calibration of gyrochronology on the handful of stars with robust age measurement to derive the age of F, G, K and early-M field stars from their rotation periods.

2 THE DATA

2.1 Observations

We determined stellar rotation rates using data from the SuperWASP camera array, located at the Observatorio del Roque de los Muchachos on La Palma, Canary Islands. With its eight cameras, SuperWASP (described in detail in Pollacco et al. 2006) has a total field of view of 640 deg^2. This extremely wide field of view provides the ability to make repeated observations of areas of the sky as large as the full Hyades cluster (10° radius, according to Perryman et al. 1998), providing densely sampled photometric data. We used fields within ∼15° of the Hyades centre ($04^h26.^m9$ + 15°52′) with a good enough sampling and a large enough time base (more than 56 d) to efficiently probe rotation periods from about a day up to about 20 d without significant field to field bias. The corresponding fields, detailed in Table 1, were observed between 25 and 100 times per night on average, with typically 5–10 min between each 30-s exposure. The most sparsely observed field, (0420+1410) was observed on 25 usable nights spanning a baseline of 56 nights in the 2008 season.

Table 1. Hyades SuperWASP fields used in this survey.

Field centre	No. of images	Usable nights	First night	Baseline (nights)
03 16′ +24 10′	3078	58	2006-09-08	135
03 17′ +23 26′	1919	61	2004-07-06	85
03 42′ +24 32′	2527	56	2006-09-16	131
03 46′ +13 14′	4721	51	2008-10-03	113
03 48′ +06 00′	4779	51	2008-10-03	113
03 51′ +17 42′	2535	56	2006-09-16	131
04 12′ +17 34′	2494	55	2006-09-16	131
04 16′ +24 10′	2555	56	2006-09-16	131
04 17′ +00 44′	4812	51	2008-10-03	113
04 17′ +23 26′	1382	47	2004-07-28	64
04 18′ +07 59′	4808	51	2008-10-03	113
04 20′ +14 10′	2181	25	2008-11-06	56
04 42′ +24 31′	2759	54	2006-09-29	140
04 46′ +13 14′	5428	52	2008-10-12	112
04 48′ +06 00′	5437	52	2008-10-12	112
04 51′ +17 41′	2733	54	2006-09-29	140
05 12′ +17 34′	2697	53	2006-09-29	140
05 18′ +07 59′	5472	52	2008-10-12	112
05 18′ +36 25′	2725	54	2006-09-29	140
05 20′ +14 09′	4462	44	2008-11-06	87
05 22′ +30 00′	2739	54	2006-09-29	140

This field yielded eight candidates, two of which yielded similar periods in another season. Given the dense sampling (more than 80 points per usable night), we do not expect any bias against short periods in this field. The shorter baseline may decrease our completeness at the long-period end of the search window. Such a bias cannot be strong because we find many variable sources with periods >18 d among the non-cluster stars in this field. Note that these fields refer to individual camera exposures and cover 62 deg^2. Since there are overlaps between them, some of the sources have been observed in different fields during different observing seasons.

2.2 Reduction and calibration

We used data reduced by the standard WASP pipeline, described in detail by Pollacco et al. (2006) and Collier Cameron et al. (2009). Each SuperWASP source is matched with NOMAD and *Hipparcos* data, providing high signal-to-noise ratio photometry in the standard *BVJHK* bands, proper motion as well as parallax when available. SuperWASP photometric data themselves are only used to look for photometric rotational modulation of the signal. Its long term rms scatter is 0.004 mag for a $V = 9.5$ star, degrading to 0.01 mag for a $V = 12$ star (Collier Cameron et al. 2009, hereafter CC09). This is achieved after a careful removal of the patterns of correlated errors, using SYSREM (Tamuz, Mazeh & Zucker 2005) as described in Collier Cameron et al. (2006). The dominant systematics are secondary extinction and temperature-dependant variations of camera focus through the night. None of these have a time-scale similar to the rotational modulation expected for 600-Myr old F, G, K or M stars. We are therefore confident that the deconvolution process does not induce spurious detections or remove genuine ones in the range of interest. A more significant bias is linked to the lunar cycle which seems, in the case of Praesepe (see Fig. 9), to dramatically increase the number of periods identified around 19.5 d, at a frequency equivalent to two-third times the lunar synodic period. As described below, this period range was removed from our sample. Saturation of SuperWASP images at $V \sim 8.5$ causes a progressive lack of periods for bright sources. At Hyades distance, this

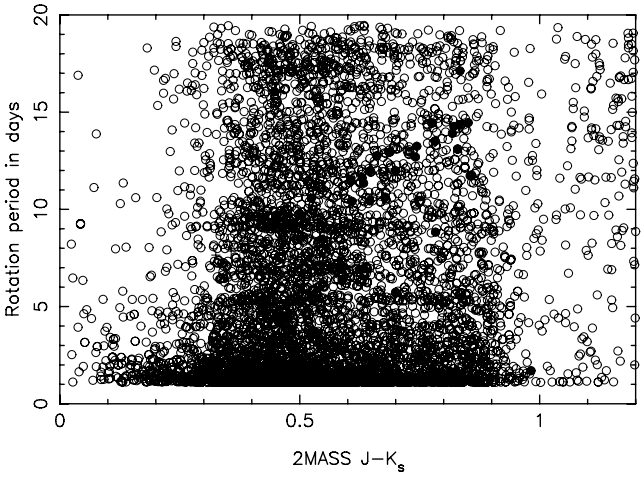

Figure 1. All sources with a good rotational signal (FAP < 0.05) detected in the fields around the Hyades cluster.

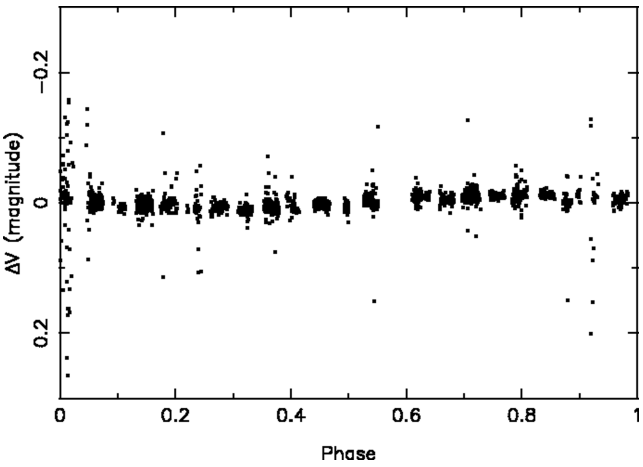

Figure 2. Folded light curve of one representative periodic variable source in the Hyades, 1SWASP J040339.03+192718.1.

translates into a biased lack of blue members with $J - K_s < 0.4$. At the red end, only the closest Hyades members are detected in V-band with enough signal to derive period. This causes a bias towards detecting only red objects brighter than the Hyades main sequence at the centre of the cluster and multiple star systems; see Fig. 5.

3 CANDIDATE SELECTION

3.1 Light-curve analysis

We used the generalized Lomb–Scargle periodogram formulation of Zechmeister & Kürster (2009) to look for quasi-sinusoidal light-curve modulation in all stars in the fields detailed in Table 1. The details of the frequency analysis and the optimized false alarm probability (FAP) calculation we used are described by CC09. We looked for signal modulation due to rotation periods between 1.1 and 20 d and selected only signals with an FAP < 0.05. We did not look for rotation periods below 1.1 d because for such short period most of the detections were caused by observational artefacts around 1 d, one night and the associated higher frequency harmonics. Lower frequency harmonics of 1 d at periods of a few days, though much less likely (see Fig. 1), are possible and we closely examined the light curves of all selected members with periods close to n days, to remove such artefacts. Rotation periods above 20 d were not investigated because our baselines were not always long enough to efficiently probe this frequency range. Moreover, very few, if any, periods over 20 d are expected in ∼600 Myr old clusters such as the Hyades. The 21 Hyades SuperWASP fields yielded 40 925 periodically variable sources out of about 1000 000 objects. As an example, we show the folded light curve of one of these variable sources in Fig. 2. Since many of these fields overlap, some variable sources have several independently determined periods from multiple observations at different seasons.

3.2 Cluster membership

Each source with a detected period was examined to determine whether or not it was a cluster member. A cluster membership probability was derived by comparing the proper motion and the apparent magnitudes of each candidate to those expected for Hyades members.

3.2.1 Proper motion

Given the wide spatial extent of the Hyades on the sky (up to 20°; Perryman et al. 1998, hereafter P98) and its proximity (46 pc; P98), it is necessary to determine the motion of each source with respect to the cluster convergent point instead of dealing directly with RA/Dec. proper motion. We therefore converted the proper motion to a component going towards the convergent point ($\mu_{\rm tan}$) and a perpendicular component ($\mu_{\rm r}$), following the method described by Reid (1992). We could then robustly estimate how the proper motion of each variable source differs from the Hyades two-dimensional space–velocity. We adopted a mean proper motion of the Hyades of $\mu_{\rm tan} = -110 \pm 0.017$ mas yr^{-1} and $\mu_{\rm r} = 0.005 \pm 0.006$ mas yr^{-1} following Reid (1992).

The next step was to compute the average proper motion of field stars, to be able to estimate how the proper motion of each variable source differs from the field two-dimensional space–velocity distribution. We used a 3σ clipped-average to eliminate Hyades stars and other extreme proper motion outliers from the field average and dispersion determination. Since Hyades stars make up for less than 0.1 per cent of the sources and populate a significantly different proper motion range (see Fig. 3), this effectively removed them from the calculation. The field proper motion distribution was determined by computing the average and dispersion of all remaining sources. The last step is to compare the relative proximity of each source to the Hyades ($f_{\rm c}$) and to the field ($f_{\rm f}$) proper motion distributions. This was carried out assuming Gaussian distribution of both population and weighted by the relative number of stars in the field, $N_{\rm f}$, and in the cluster, $N_{\rm c}$, to take into account that there are many more field stars than cluster stars in our sample. $N_{\rm c}$ was determined by running the full membership routine recursively until $N_{\rm c}$, defined as the number of sources with a cluster membership probability over 50 per cent, converged. $N_{\rm f}$ is the size of the sample minus $N_{\rm c}$. The related equations are the following:

$$f_{\rm f} = \frac{N_{\rm f}}{2\pi\Sigma_{{\rm f}\alpha}\Sigma_{{\rm f}\delta}} \exp\left[-\frac{(\mu_{\alpha i} - \mu_{{\rm f}\alpha})^2}{2\Sigma_{{\rm f}\alpha}^2} - \frac{(\mu_{\delta i} - \mu_{{\rm f}\delta})^2}{2\Sigma_{{\rm f}\delta}^2}\right], \quad (1)$$

with mean proper motion $\mu_{{\rm f}\alpha} = 2.85$ mas yr^{-1}, $\mu_{{\rm f}\delta} = -8.86$ mas yr^{-1} and dispersion $\Sigma_{{\rm f}\alpha} = 10.48$ mas yr^{-1}, $\Sigma_{{\rm f}\delta} = 10.78$ mas yr^{-1}. Since the intrinsic spread in the proper motions of the cluster members is smaller than the measurement errors, the density function for cluster members depends on the uncertainties in the proper motion

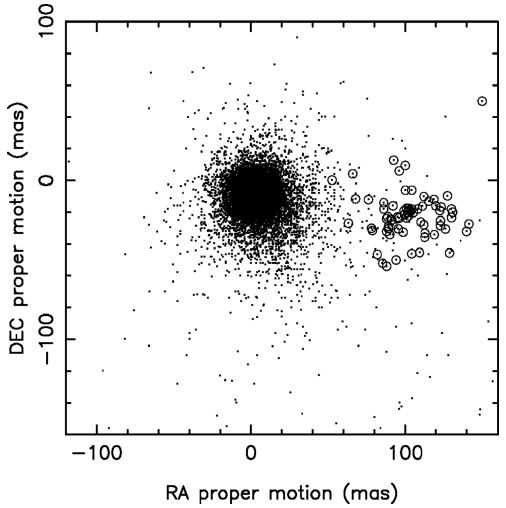

Figure 3. Proper motion in RA and Dec. of all sources with identified rotational modulation signal in our survey. Objects identified as Hyades members owing to their proper motion and apparent magnitude are circled.

components $\sigma_{\mathrm{tan}i}$ and σ_{ri} for each individual star:

$$f_{\mathrm{c}} = \frac{N_{\mathrm{c}}}{2\pi\sigma_{\mathrm{ctan}}\sigma_{\mathrm{cr}}} \exp\left[-\frac{(\mu_{\mathrm{tan}i}-\mu_{\mathrm{ctan}})^2}{2\sigma_{\mathrm{tan}i}^2} - \frac{(\mu_{ri}-\mu_{\mathrm{cr}})^2}{2\sigma_{ri}^2}\right]. \quad (2)$$

Following Girard et al. (1989), the cluster membership probability for an individual star is

$$p = \frac{f_{\mathrm{c}}}{f_{\mathrm{c}}+f_{\mathrm{f}}}.$$

Since $\sigma_{\mathrm{tan}i}$ and σ_{ri} are much smaller than $\Sigma_{\mathrm{f}\alpha}$ and $\Sigma_{\mathrm{f}\delta}$, f_{c} decreases much faster than f_{f} and stars far from both distributions usually have $p = 0$. Because the difference between the field and the cluster proper motion is much greater than their dispersions, there is however a locus in proper motion space where obvious outliers of both distributions could be selected as cluster members. We eliminated two such objects manually at the end of the selection process. As in CC09, we extended this definition of cluster membership to include information on the apparent magnitude.

3.2.2 Apparent magnitude

The same rationale was applied to determine whether the colour and apparent magnitude of each source was closer to the field distribution or to the colour–magnitude relation expected for Hyades stars. For the Hyades, this relation was derived using the Pinsonneault et al. (2004) isochrone for [M/H] = +0.1 and age = 600 Myr that has been empirically calibrated to fit the Hyades. We determined the expected apparent K_{s} magnitude for Hyades members of a given $V - K_{\mathrm{s}}$ colour and compared it to the observed magnitude of each object. Note that all near-infrared magnitudes used in this paper are Two Micron All-Sky Survey (2MASS) magnitudes. *Hipparcos* parallax information was available for only 0.4 per cent of the overall number of sources, but eventually for more than 30 per cent of the selected members (mainly because Hyades stars are much closer than the average field stars and are more likely to have been observed by *Hipparcos*). This was directly converted into apparent K_{s} magnitudes and compared to the observed K_{s} magnitude of the source. In most cases, however, we do not have the parallax information and we are forced to rely on the average Hyades distance, associated with an arbitrary large – and conservative – dispersion (0.5 mag, assuming a 15–20 pc cluster extent and ensuring we do not clip out any good candidate with this approximate selection) of the expected apparent magnitude to account for the large distance range where Hyades members can be found. This integrates into the membership estimation as follows.

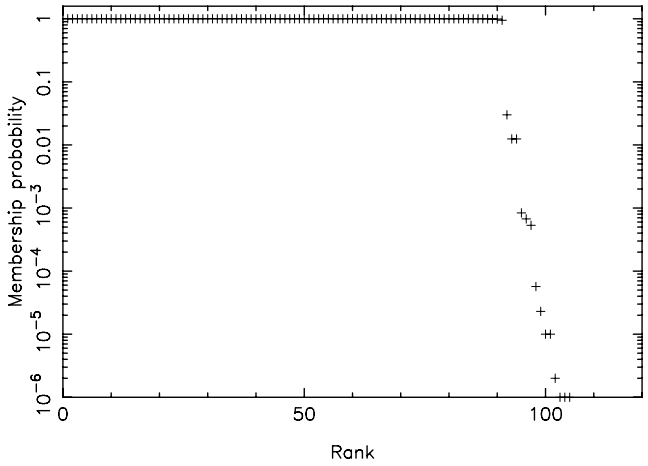

Figure 4. Ranked cluster membership probability for the 120 most probable Hyades cluster members variables sources.

We multiply the probability densities for the K_{s} magnitude offset from the field distributions with the field proper motion probability density from equation (1) above before obtaining the final membership probability p:

$$g_{\mathrm{f}} = \frac{f_{\mathrm{f}}}{\sqrt{2\pi}\Sigma_{\mathrm{f}K}} \exp\left(-\frac{\delta K_{\mathrm{f}i}^2}{\Sigma_{\mathrm{f}K}^2}\right), \quad (3)$$

and similarly for the cluster probability density, we obtain

$$g_{\mathrm{c}} = \frac{f_{\mathrm{c}}}{\sqrt{2\pi}\Sigma_{\mathrm{c}K}} \exp\left[-\frac{(K_i - K_{\mathrm{isochrone}})^2}{\Sigma_{\mathrm{c}K}^2}\right]. \quad (4)$$

The combined membership probability for an individual star is then

$$p = \frac{g_{\mathrm{c}}}{g_{\mathrm{c}}+g_{\mathrm{f}}}.$$

Given the relatively large proper motion of the Hyades members and the large offset from the field population average proper motion (over 100 mas yr^{-1} difference from the field, typically 10 times the proper motion measurement scatter, see Fig. 3), the proper motion criterion is highly selective, while the large spatial extent (and hence depth) of the Hyades makes the apparent magnitude criterion much less accurate. We therefore used a very conservative magnitude selection parameter, with a large $\Sigma_{\mathrm{f}K}$ of 0.5 mag, to eliminate only the candidates far from the expected Hyades magnitudes and used proper motion as our main selection criterion. The resulting membership probability distribution is largely bimodal, with objects clustering at probability of 1 (Hyades members) or 0 (field sources), see Fig. 4. We intended to select all sources with $p > 50$ per cent as cluster members, but in practical there is no variable source in our Hyades sample with $94 > p > 50$ per cent.

This automated selection yielded 91 variable sources identified as cluster members. This sample is far from being a complete census of rotation periods of the hundreds of Hyades stars, and we put more emphasis on clearing contamination than on increasing the sample size. Since our FAP selection cut for the period detection is 5 per cent, our sample is nevertheless expected to contain a few spurious periods and more are expected because of possible instrumental artefacts. We therefore visually examined their light curves and periodograms, and computed their autocorrelation functions (ACF)

of the light curves using an inverse variance-weighted adaptation of the discrete correlation function method of Edelson & Krolik (1988). We retained 83 cluster members whose light-curve ACFs showed clear periodic structure, and whose periodogram-selected periods agreed with the time lag of the first peak in the ACF. To minimize any human bias during this step of the analysis, we did not check the objects' colour and did not know beforehand whether or not they agreed with the colour–period relation described in next section. As explained above, we also rejected two of our selected members because their proper motions, even though much closer to the Hyades proper motion than to the field, were still more than 10σ away from the Hyades locus. Among the remaining 81 Hyades members with periods detected, 11 were independently detected twice (leaving 70 independent members), during two different observing seasons. The periods at the two epochs matched very well for nine of them, with a scatter of the difference of 0.09 d (i.e. 0.8 per cent of their average period), giving a good estimate of our period measurement accuracy. We assigned the average period of the observations to these stars. The two remaining objects (1SWASP J044735.33+145320.7 and 1SWASP J051109.69+154857.5) were detected during one season at a higher frequency harmonic (1/2 and 1/6 of the period) than the other season. The lower frequency folded light curves appeared much more reliable than the harmonics and were retained. We finally obtained a catalogue of 70 Hyades cluster members with reliable periods measured with SuperWASP. They are shown in Table 2, Figs 5 and 6. Additional optical photometry and cross-identification with known cluster members is shown in the Appendix A.

4 PERIOD-COLOUR RELATION

4.1 The relation

To derive a clean period–colour relation, we selected the reliable candidates which sit in the $0.2 < J - K_s < 0.82$ colour range, where Hyades stars have converged towards an identifiable colour–period relation. Since we have a large sample, we used a recursive clipped average selection to eliminate those objects that are likely outliers (binary systems, mistaken cluster members or instrumental period artefacts). A least-squares linear fit was first performed on all sources in this colour range. Their dispersion around this first estimate of the relation was calculated and all candidates more than 2σ away from this relation were removed. It turns out that this only removed the two members identified as spectroscopic binaries that we could have removed manually. Since we also used the same method, with the same parameters, to remove outliers on our Praesepe sample (see next section), for which information on spectroscopic binarity was not available, this allowed a consistent analysis of both clusters samples. The two Hyades outliers that are spectroscopic binaries are 1SWASPJ043225.66+130647.6 (HD286839, orbital period of 1.48 d; Mermilliod, Mayor & Udry 2009) and 1SWASPJ044912.98+244810.2 (HD283882, SB2 with an orbital period of 11.93 d; Mermilliod et al. 2009). A new least-squares linear fit was performed on the remaining sources to derive the final relation, with a smaller dispersion (see Fig. 7). We also tried to fit a quadratic relation through our data, but it did not significantly increase the correlation coefficient of the fit. We therefore used the simpler linear fit to find the period–colour relation.

The derived relation is the following:

$$P = 11.401 + 12.652 * (J - K_s - 0.631). \quad (5)$$

Though the 0.58-d dispersion of periods around the relation is smaller than the dispersion observed around more complex colour–period relation in younger clusters such as M34, M35 and M37 (Hartman et al. 2009; Meibom et al. 2009), it is significantly higher than the 0.19-d dispersion observed around Coma cluster relation by CC09 using the same methods. As explained above, we used objects whose periods have been detected during two different seasons to estimate that the error on the period measurement is about 0.1 d. This means that the relatively large spread of periods for a given colour that we observe in the Hyades is not an observational bias but is real. It could not be caused by differential rotation because this affects significantly only F and G stars (Barnes 2005; Reiners 2006) while the spread in periods is observed on the FGKM spectral range (see Fig. 7). Theoretical models of stellar spin-down (see Kawaler 1988; Collier Cameron & Jianke 1994; Irwin & Bouvier 2009, for instance) do predict that by 600-Myr stellar spin has almost, but not completely, converged for stars more massive than $0.25\,M_\odot$. However, this does not explain the difference between Coma and the Hyades, which is discussed more extensively in Section 5, and includes data on Praesepe cluster.

4.2 Comparison to Radick 87 and 95 members

Fig. 8 shows our new SuperWASP periods for Hyades cluster members together with previous objects measured by Radick et al. (1987, 1995, hereafter R87–95). The scatter of the R87–95 periods appears larger, perhaps because of differential rotation on these higher mass objects or perhaps because the time sampling of R87–95, optimized towards monitoring years-long photometric variability and not day-long rotational periods causes larger errors on period measurements. Direct comparison with our data is, unfortunately, difficult since most of the R87–95 are blue, bright stars that are saturated in SuperWASP images. We fitted a linear colour–period relation through the full SuperWASP+R87–95 data and obtained a quite similar relation:

$$P' = 10.189 + 13.091(J - K_s - 0.536) \quad (6)$$

with a dispersion of 0.79 d around the relation, which is shown, together with SuperWASP-only data in Fig. 8.

We also tried to fit a quadratic relation, but this did not improve the correlation. By eye, it seems there could be a break in the colour–period relation around $J - K_s = 0.43$. We therefore tried to fit a two-part piecewise linear relation through the data, but again this did not improve the correlation coefficient: the apparent break in the relation is likely caused by the increased scatter of R87–95 data. We consequently used the simple linear fit. However, given the small difference between the relations in equations (5) and (6), in the following we use equation (5), from SuperWASP-only data, to compare with SuperWASP-only data from the Praesepe and Coma clusters.

5 PRAESEPE

5.1 Observations, reduction and candidate selection

Our analysis of the SuperWASP fields overlapping Praesepe cluster (also known as M44 or Melotte 88) followed the same strategy as our analysis of the Hyades that has been described in the previous section. Table 3 details the two SuperWASP fields with a good time sampling (60–70 images per night) and a long enough baseline (130 nights) that we found within 10° of the cluster centre ($08^h40\overset{m}{.}4\ +19°41'$). We looked for all rotational variables with

Table 2. Hyades members with SuperWASP rotation periods. Period is in days and if the object has been identified on two different seasons, the period given is the average of the two periods whose difference is indicated in exponent. Proper motion and parallax are in mas. Dist. is the distance to the cluster centre in degrees, and Proba. is the membership probability. $J - K_s$ is a 2MASS colour. X-ray traces whether or not Stern, Schmitt & Kahabka (1995) reported X-ray activity.

Swasp ID	USNO ID	X-ray	Period	$J - K_s$	K_s	V	Dist.	Proper Motion(μ_{RA}, $\mu_{Dec.}$)	prlx	Proba.
1SWASPJ033734.97+212035.4	1113-0041831	Yes	10.57	0.524	7.12	9.3	12.4	141.5 ± 1.7, −27.3 ± 1.3	25.18	1.00
1SWASPJ034347.07+205136.4	1108-0041451	No	12.30	0.871	9.61	–	10.9	140.0 ± 1.0, −32.0 ± 1.0	–	1.00
1SWASPJ035234.31+111538.6	1012-0033507	No	13.29	0.858	9.01	–	10.2	166.0 ± 15.0, −10.0 ± 1.0	–	1.00
1SWASPJ035453.20+161856.3	1063-0039925	Yes	$6.04^{0.013}$	0.905	9.06	–	7.7	130.0 ± 2.0, −18.0 ± 2.0	–	1.00
1SWASPJ035501.43+122908.1	1024-0045401	–	11.66	0.607	7.57	10.0	8.9	127.5 ± 2.1, −9.6 ± 1.5	25.62	1.00
1SWASPJ040339.03+192718.1	1094-0044958	No	$11.45^{0.075}$	0.606	7.60	10.2	6.0	119.0 ± 2.3, −34.1 ± 1.8	23.27	1.00
1SWASPJ040525.67+192631.7	1094-0045433	No	$13.51^{0.016}$	0.782	8.11	11.7	5.6	123.0 ± 3.2, −28.4 ± 2.2	15.76	1.00
1SWASPJ040634.62+133256.8	1035-0040066	No	16.68	0.891	9.09	–	6.0	112.0 ± 2.0, −10.0 ± 2.0	–	1.00
1SWASPJ040701.22+152006.0	1053-0044486	No	$11.98^{0.036}$	0.700	7.66	10.3	5.1	122.6 ± 2.0, −18.9 ± 1.5	24.19	1.00
1SWASPJ040743.19+163107.6	1065-0042472	No	12.30	0.594	7.51	9.9	4.6	123.0 ± 1.6, −25.2 ± 1.2	19.67	1.00
1SWASPJ040811.02+165223.3	1068-0041870	No	13.63	0.833	7.93	11.1	4.5	128.8 ± 5.5, −45.6 ± 7.0	–	1.00
1SWASPJ040826.66+121130.6	1021-0043331	No	12.96	0.772	8.05	11.3	6.6	115.3 ± 2.8, −13.0 ± 2.3	25.93	1.00
1SWASPJ040836.21+234607.0	1137-0048046	–	9.35	0.517	7.32	9.4	7.9	120.4 ± 0.6, −43.9 ± 0.7	–	1.00
1SWASPJ041127.64+155931.8	1059-0051230	No	$1.79^{0.008}$	0.866	9.94	14.9	3.9	120.0 ± 4.0, −16.0 ± 3.0	–	1.00
1SWASPJ041510.33+142354.5	1043-0041060	No	13.91	0.818	8.13	12.7	3.9	118.8 ± 4.6, −11 ± .9 ± 3.9	27.31	1.00
1SWASPJ041633.47+215426.8	1119-0053591	No	10.26	0.426	7.27	9.1	5.4	105.6 ± 1.3, −37.5 ± 1.1	19.07	1.00
1SWASPJ041725.14+190147.4	1090-0048172	No	12.95	0.688	7.91	11.0	2.9	112.0 ± 6.3, −27.8 ± 8.1	–	1.00
1SWASPJ041728.13+145403.9	1049-0042422	Yes	2.35	0.850	9.62	14.4	3.1	104.0 ± 6.0, −18.0 ± 2.0	–	1.00
1SWASPJ042322.85+193931.1	1096-0050945	Yes	9.90	0.571	7.15	9.4	2.7	98.5 ± 1.7, −32.5 ± 1.4	16.50	1.00
1SWASPJ042325.28+154547.2	1057-0062216	No	12.38	0.699	7.49	10.6	1.6	126.2 ± 2.9, −30.5 ± 2.4	21.26	1.00
1SWASPJ042350.70+091219.5	992-0039564	Yes	5.33	0.891	8.23	13.1	7.9	104.0 ± 3.0, −6.0 ± 1.0	–	1.00
1SWASPJ042359.13+164317.7	1067-0045253	No	$17.14^{0.320}$	0.860	8.56	12.8	0.8	110.0 ± 2.0, −26.0 ± 1.0	–	1.00
1SWASPJ042416.93+180010.4	1080-0063868	No	$11.60^{0.039}$	0.630	7.52	10.0	1.1	112.7 ± 2.4, −33.2 ± 1.9	19.31	1.00
1SWASPJ042500.18+165905.8	1069-0045244	No	11.77	0.656	7.83	10.4	0.5	95.8 ± 2.8, −23.7 ± 2.6	–	1.00
1SWASPJ042514.54+185824.9	1089-0051192	Yes	10.84	0.888	8.70	12.8	1.9	92.0 ± 4.0, −28.02.0	–	1.00
1SWASPJ042547.55+180102.2	1080-0064462	Yes	8.46	0.547	6.77	–	0.9	112.6 ± 2.4, −35.7 ± 2.0	20.79	1.00
1SWASPJ042642.81+124111.7	1026-0052108	Yes	12.61	0.794	7.03	–	4.4	123.4 ± 3.9, −16.7 ± 2.5	29.09	1.00
1SWASPJ042648.25+105215.9	1008-0039886	Yes	$10.40^{0.075}$	0.646	6.88	9.4	6.2	111.0 ± 1.8, −16.2 ± 1.3	24.11	1.00
1SWASPJ042725.34+141538.3	1042-0043123	Yes	12.776	0.661	7.71	10.3	2.8	103.2 ± 1.4, −19.4 ± 1.6	–	1.00
1SWASPJ042747.03+142503.8	1044-0042884	Yes	9.70	0.546	7.35	9.5	2.7	101.4 ± 1.9, −20.0 ± 1.5	19.00	1.00
1SWASPJ042828.78+174145.1	1076-0062237	Yes	2.42	0.881	7.71	12.1	0.7	105.1 ± 16.3, −20.1 ± 8.3	–	1.00
1SWASPJ043033.88+144453.1	1047-0044652	No	18.41	0.852	9.71	–	2.5	102.0 ± 12.0, −22.0 ± 2.0	–	1.00
1SWASPJ043034.87+154402.3	1057-0063658	Yes	8.73	0.519	6.82	8.8	1.6	99.5 ± 11.1, −21.5 ± 1.1	–	1.00
1SWASPJ043152.40+152958.3	1054-0052709	No	13.13	0.772	7.89	11.3	2.0	100.7 ± 14.5, −23.4 ± 3.2	19.12	1.00
1SWASPJ043225.66+130647.6	1031-0059808	Yes	1.48	0.769	7.65	11.1	4.2	102.3 ± 13.5, −18.7 ± 12.7	17.75	1.00
1SWASPJ043323.75+235927.0	1139-0053890	Yes	17.55	0.885	8.03	–	7.1	94.0 ± 12.0, −50.0 ± 1.0	–	1.00
1SWASPJ043327.00+130243.6	1030-0056878	No	16.29	0.861	8.82	13.4	4.3	108.0 ± 13.0, −18.0 ± 2.0	–	1.00
1SWASPJ043337.18+210903.0	1111-0054738	No	12.69	0.741	7.69	10.6	4.4	109.2 ± 12.2, −45.3 ± 1.7	26.74	1.00
1SWASPJ043411.14+113328.4	1015-0040520	Yes	11.03	0.831	8.06	11.3	5.8	100.7 ± 12.2, −17.5 ± 1.5	–	1.00
1SWASPJ043548.51+131717.0	1032-0063919	Yes	13.36	0.863	9.87	14.9	4.4	92.0 ± 12.0, −16.0 ± 1.0	–	1.00
1SWASPJ043605.26+154102.4	1056-0061021	No	9.47	0.487	7.37	9.3	2.6	95.0 ± 11.0, −23.1 ± 1.2	–	1.00
1SWASPJ043950.97+124342.5	1027-0058818	Yes	10.85	0.609	7.48	10.0	5.4	102.0 ± 12.2, −17.61.6	23.33	1.00
1SWASPJ044127.81+140434.1	1040-0045181	–	1.28	0.865	8.71	13.3	4.6	86.0 ± 13.0, −18.0 ± 4.0	–	1.00
1SWASPJ044128.75+120033.7	1020-0044793	No	18.00	0.859	8.75	13.0	6.2	86.0 ± 12.0, −14.0 ± 5.0	–	0.999
1SWASPJ044129.67+131316.3	1032-0065593	No	15.42	0.849	7.51	11.2	5.2	99.1 ± 12.7, −19.22.3	–	1.00
1SWASPJ044142.98+082620.0	984-0050517	–	8.02	0.879	10.06	14.7	9.4	100.0 ± 14.0, −6.0 ± 2.0	–	1.00
1SWASPJ044315.69+170408.7	1070-0053038	Yes	10.31	0.606	7.40	9.9	3.9	95.4 ± 11.6, −30.4 ± 1.3	–	1.00
1SWASPJ044618.79+033810.7	936-0059947	No	13.25	0.744	7.83	11.0	14.3	92.5 ± 12.8, 12.9 ± 2.1	23.05	1.00
1SWASPJ044630.38+152819.3	1054-0056655	Yes	7.95	0.360	6.74	8.3	5.0	91.3 ± 11.4, −24.7 ± 1.0	21.08	1.00
1SWASPJ044718.51+062711.6	964-0047473	No	14.44	0.776	7.87	12.0	11.7	99.9 ± 15.0, 9.5 ± 2.8	–	1.00
1SWASPJ044800.88+170321.6	1070-0054253	Yes	10.77	0.840	7.37	11.7	5.0	89.1 ± 12.1, −30.22.1	–	1.00
1SWASPJ044830.61+162319.0	1063-0051391	–	15.69	0.872	8.54	12.6	5.2	78.0 ± 16.0, −30.0 ± 3.0	–	1.00
1SWASPJ044842.13+210603.6	1111-0060275	Yes	9.69	0.450	7.07	9.1	6.5	81.8 ± 15.0, −46.4 ± 4.7	19.41	1.00
1SWASPJ044912.98+244810.2	1148-0059776	Yes	6.9	0.626	6.96	9.5	9.3	85.2 ± 11.6, −52.0 ± 11.2	20.11	1.00
1SWASPJ044952.11+060633.6	961-0047586	No	17.12	0.834	9.63	14.5	12.3	96.0 ± 15.0, 6.0 ± 2.0	–	1.00
1SWASPJ045000.70+162443.5	1064-0050763	No	11.98	0.646	7.84	10.7	5.5	89.2 ± 12.2, −28.9 ± 1.7	–	1.00
1SWASPJ045102.41+145816.5	1049-0049205	–	$13.14^{0.102}$	0.829	7.97	11.9	6.2	88.0 ± 13.0, −32.0 ± 6.0	–	1.00
1SWASPJ045223.53+185948.9	1089-0058167	Yes	11.34	0.633	7.74	10.3	6.3	78.6 ± 12.3, −31.4 ± 1.5	21.55	1.00
1SWASPJ045223.86+104309.9	1007-0045668	–	9.88	0.860	8.77	13.0	8.9	76.0 ± 14.0, −12.0 ± 5.0	–	1.00
1SWASPJ050540.37+062754.6	964-0053308	No	10.41	0.609	7.52	9.9	14.2	66.0 ± 12.1, 4.2 ± 1.1	19.24	1.00
1SWASPJ051109.69+154857.5	1058-0068980	–	14.94	0.872	8.10	12.3	10.7	63.2 ± 16.3, −26.8 ± 18.3	–	0.992
1SWASPJ051119.30+075432.0	979-0066501	–	13.23	0.696	8.30	11.2	14.2	52.5 ± 16.3, 0.2 ± 18.1	–	0.947

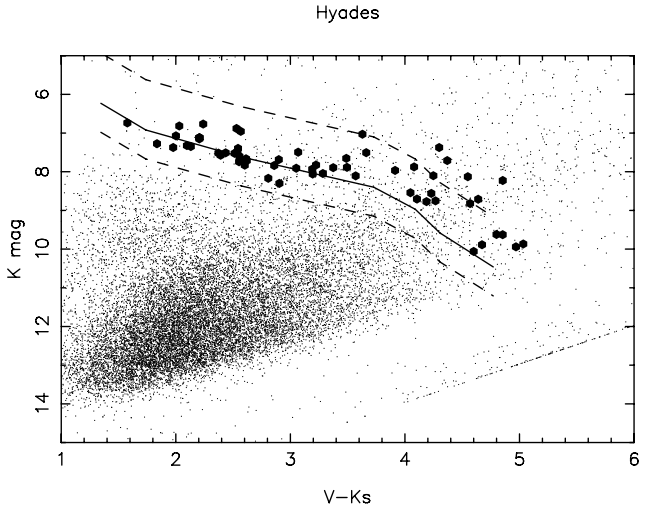

Figure 5. Colour–magnitude diagram of field stars (dots) and Hyades-selected members (black circles). The Hyades main sequence at cluster centre (42 pc) is shown as a black line. The Hyades main sequences at 25 and 65 pc are shown as dashed lines.

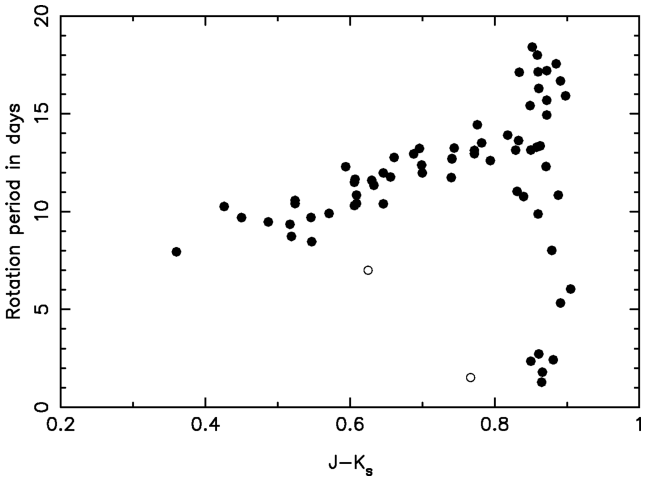

Figure 6. $J - K_s$ colour–period plot of all selected Hyades members. The two outliers in hollow circles are known spectroscopic binaries.

periods between 1.1 and 20 d in these fields using the light-curve analysis described in Section 3.1. This yielded 3324 rotational variables.

5.1.1 Candidate selection

As can be seen in Fig. 9, there is a significant bias in these data that causes overnumerous detections of periods greater than 18 d. A close examination of these light curves confirmed that this was likely due to an instrumental/observational bias on one of the detectors. We consequently eliminated all these sources for the rest of the study. The overdensities visible on Fig. 9 around 8 and 13 d are likely due to windowing in SWASP time-sampling, but only one candidate was selected at a nearby period, 1SWASP J083627.86+210716.2. This period however appears reliable since it has been independently detected on the two fields. Following again the same procedure as we used for the Hyades, we selected candidates closer to the colour and proper motion of Praesepe ($\mu_\alpha = -35.99 \pm 4$ mas yr^{-1}; $\mu_\delta = -12.92 \pm 4$ mas yr^{-1}; Loktin & Beshenov 2003; Kraus & Hillenbrand 2007). Since Praesepe is not as nearby nor as extended on the sky as the Hyades, we performed a simple comparison of RA/Dec. proper motion and not a comparison of proper motion tangential and perpendicular to the convergent point as we did for the Hyades. The overall membership probability determination from proper motion and apparent magnitude is otherwise identical to what we did for the Hyades and described in Section 3. The expected colour–magnitude relation for clusters members was derived using the isochrones of Pinsonneault et al. (2004), for an age of 600 Myr and a metallicity of [M/H] = +0.1 (+0.14 for Praesepe according to Scholz & Eislöffel 2007).

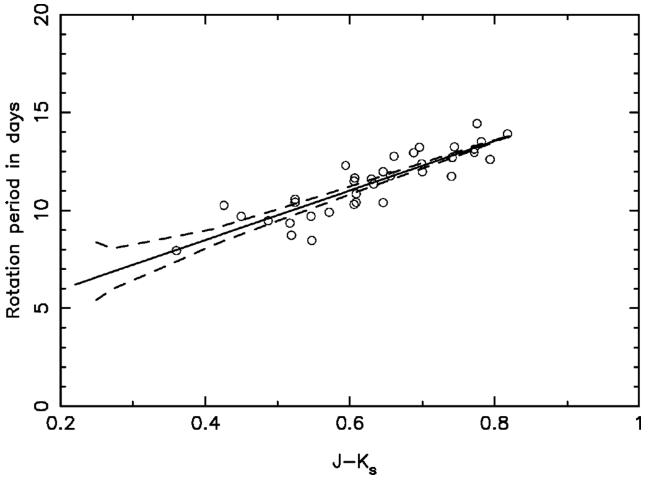

Figure 7. $J - K_s$ colour–period plot of Hyades members that are used to derive the colour–period relation (black line). The dashed lines represent the expected spread in periods caused by differential rotation (see CC09 for details).

This analysis yielded 71 reliable Praesepe cluster members with a membership probability over 50 per cent. These objects are shown in Fig. 10 and additional optical photometry and cross-identification with known cluster members is shown in the Appendix A. Since the proper motion locus of Praesepe is closer to the field stars' locus, the membership probability distribution shown on Fig. 11 is not as bimodal as the distribution obtained for the Hyades but still non-ambiguously distinguishes between cluster members and others. One of this selected members had $V - K_s$ colours and a K_s magnitude compatible with an early M-dwarf cluster member but $J - K_s$ colours and magnitudes typical of a field G dwarf. Since $J - K_s$ colour is more reliable, this object was rejected as a probable field star. Overall Praesepe data was of lower quality than the average Hyades data, first because of a slightly sparser time sampling and secondly, because of the persistence of some moon-related red noise even after decorrelation of data. A careful analysis of each light curve eliminated 12 of the candidates whose derived periods appeared spurious. Again this selection was done without the knowledge of the colour to avoid any human bias towards removing preferentially candidates that would not fit the relation. Six objects turned out to have been detected twice, at about the same period in both field. As for the Hyades, we assigned the average of the two periods to these objects. We use the scatter of the difference of both periods, 0.14 d, as an estimate of our error on period measurement. Our Praesepe analysis uses the 52 independent remaining cluster members with reliable periods visible on Table 4 and Fig. 12.

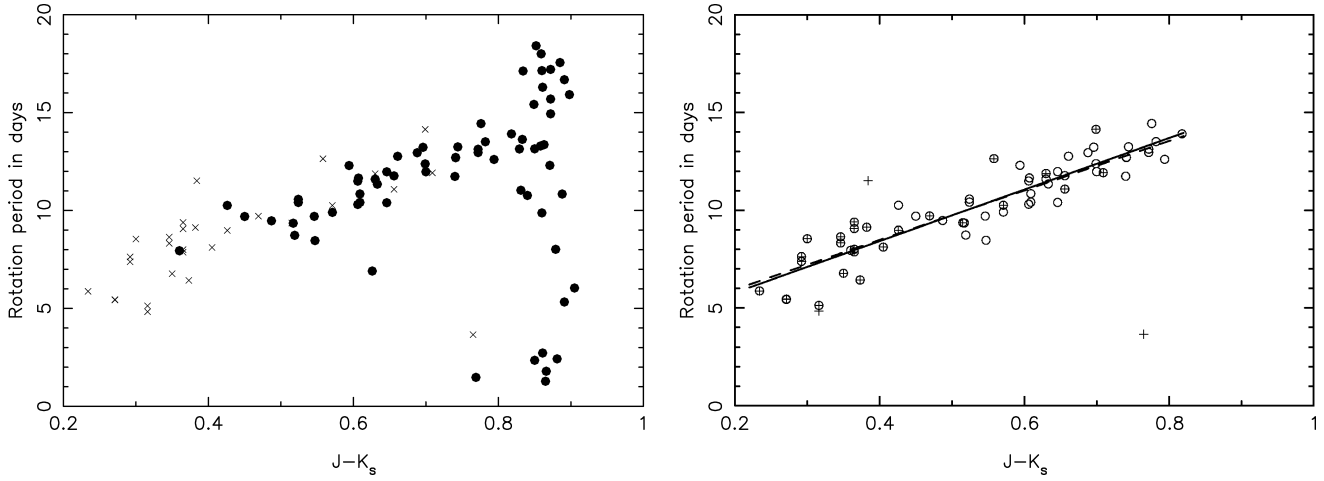

Figure 8. Left: $J - K_s$ colour–period plot of all SuperWASP-selected Hyades members (black dots) and rotational periods previously observed by Radick et al. (1987, 1995) (crosses). Right: stars used to derive the linear fit with SuperWASP and R87–95 data (black line) are circled. The SuperWASP-only relation is shown in dashed line.

Table 3. Praesepe superWASP fields used in this survey.

Field centre	No. of images	Usable nights	First night	Baseline (nights)
08 42′ +24 18′	3963	59	2006-11-26	130
08 52′ +17 35′	4144	60	2006-11-26	130

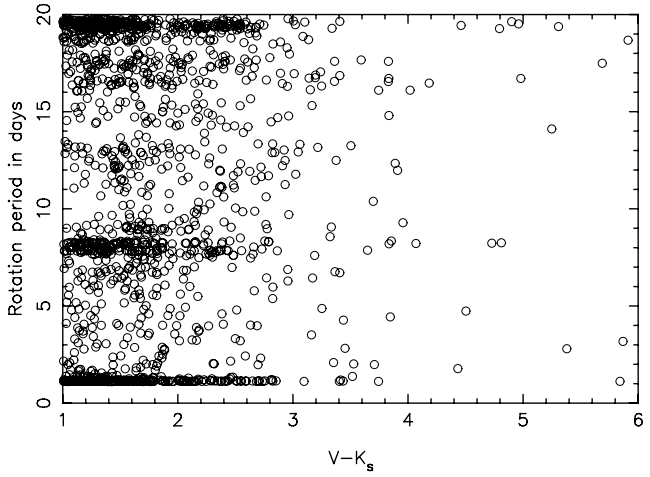

Figure 9. All sources with a good signal-to-noise ratio rotational signal detected in the fields around Praesepe cluster.

5.2 Period–colour relation

As for the Hyades, we tried to fit a linear relation, a quadratic law and two linear laws (for $J - K_s < 0.43$ and $J - K_s > 0.43$), and the resulting correlation coefficients were very similar. We therefore favoured the simpler linear fit because it has fewer free parameters and fits well to the data.

We derived the colour–period relation in a similar way as for the Hyades, using all members with $0.2 < J - K_s < 0.82$, and making a linear fit after clipping out the five outliers above and below the relation in this colour range. Note that two of them, 1SWASP J083722.23+201037.0 and 1SWASP J084005.72+190130.7, have been identified at a period that is half of the expected period. It is likely that these objects rotation periods actually sit on

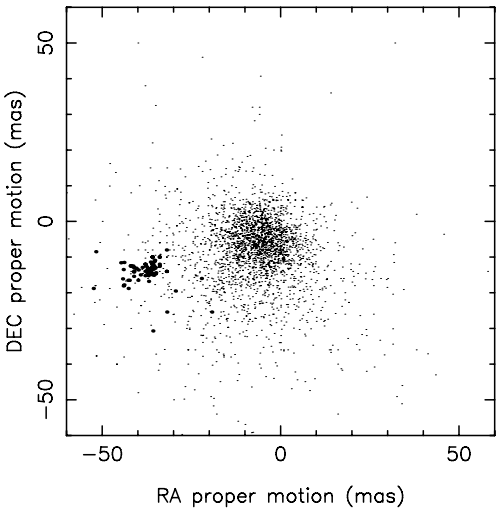

Figure 10. Proper motion in RA and Dec. of all sources with identified rotational modulation signal in our survey around Praesepe. Large dots are objects identified as cluster member owing to their proper motion and apparent magnitude.

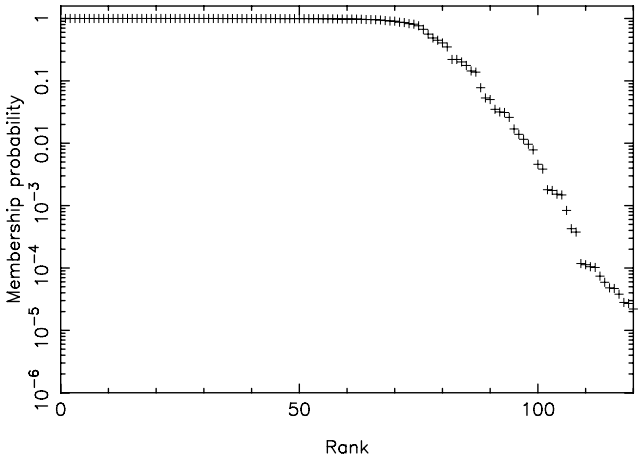

Figure 11. Ranked cluster membership probability for the 120 most probable Praesepe cluster member variables sources.

Table 4. Praesepe members with SWASP rotation periods. Period is in days and if the object has been identified on two different seasons, the period given is the average of the two periods whose difference is indicated in exponent. Proper motion and parallax are in mas. Dist. is the distance to the cluster centre in degrees, and Proba. is the membership probability. $J - K_s$ is a 2MASS colour.

SWASP ID	USNO ID	Period	$J - K_s$	K_s	V	Dist.	Proper Motion(μ_{RA}, $\mu_{Dec.}$)	Proba.
1SWASP J083141.93+260641.0	1161-0156334	13.16	0.738	10.79	13.7	6.7	-42.8 ± 5.6, -16.5 ± 5.6	1.000
1SWASP J083554.98+224611.3	1127-0193591	9.31	0.532	10.23	12.7	3.3	-29.5 ± 5.2, -19.5 ± 5.2	0.928
1SWASP J083622.69+191129.3	1091-0164534	9.83	0.506	10.25	12.4	1.1	-39.9 ± 6.0, -13.6 ± 6.1	0.998
1SWASP J083627.81+175453.4	1079-0203318	6.91	0.315	9.40	10.9	2.0	-36.5 ± 1.1, -11.4 ± 1.1	0.999
1SWASP J083627.86+210716.2	1111-0173917	$13.09^{0.123}$	0.757	10.96	13.8	1.7	-36.0 ± 1.0, -10.0 ± 1.0	0.979
1SWASP J083628.30+201342.8	1102-0162570	10.25	0.541	10.44	12.7	1.1	-44.3 ± 6.3, -16.1 ± 6.3	0.998
1SWASP J083648.96+191526.4	1092-0164565	7.41	0.396	9.68	11.3	0.9	-36.2 ± 2.3, -12.8 ± 1.3	1.000
1SWASP J083657.82+213355.9	1115-0175522	$13.27^{0.111}$	0.834	11.12	14.1	2.0	-42.1 ± 6.3, -12.5 ± 6.3	1.000
1SWASP J083711.48+194813.2	1098-0164221	8.84	0.389	9.68	11.1	0.8	-35.4 ± 0.7, -12.8 ± 0.7	0.977
1SWASP J083718.29+194156.3	1096-0163761	8.90	0.373	9.80	11.6	0.7	-37.1 ± 1.9, -15.2 ± 1.9	0.999
1SWASP J083722.23+201037.0	1101-0161763	3.91	0.384	9.80	11.3	0.9	-36.0 ± 0.7, -14.5 ± 0.9	0.990
1SWASP J083727.54+193703.1	1096-0163804	8.68	0.446	9.80	11.5	0.7	-34.0 ± 1.9, -12.6 ± 1.9	0.998
1SWASP J083733.07+183915.5	1086-0168273	7.59	0.338	9.28	10.5	1.2	-37.5 ± 1.2, -14.3 ± 1.4	0.999
1SWASP J083735.77+205927.5	1109-0174003	$10.09^{0.428}$	0.636	10.25	12.9	1.5	-32.0 ± 4.0, -14.0 ± 3.0	0.994
1SWASP J083746.41+193557.5	1095-0163684	9.50	0.481	10.24	12.3	0.6	-41.3 ± 6.3, -12.9 ± 6.3	0.996
1SWASP J083747.39+190624.8	1091-0164888	9.30	0.464	10.20	11.9	0.8	-35.6 ± 2.0, -15.1 ± 2.0	0.911
1SWASP J083857.23+201053.6	1101-0162189	11.78	0.764	10.71	13.7	0.6	-41.2 ± 6.4, -15.4 ± 6.4	1.000
1SWASP J083902.28+191934.4	1093-0163918	9.42	0.471	10.25	12.3	0.5	-44.1 ± 6.3, -13.5 ± 6.3	0.998
1SWASP J083921.54+204529.4	1107-0171494	9.11	0.450	10.02	11.6	1.1	-35.0 ± 1.3, -14.4 ± 1.3	0.826
1SWASP J083930.44+200408.6	1100-0163760	7.02	0.333	8.80	10.2	0.4	-35.7 ± 0.8, -13.4 ± 0.7	0.992
1SWASP J083935.53+185236.8	1088-0166993	6.29	0.328	9.32	10.6	0.8	-37.3 ± 1.2, -13.1 ± 1.5	0.999
1SWASP J083945.78+192201.1	1093-0164074	5.90	0.306	9.25	10.8	0.4	-35.3 ± 0.9, -12.8 ± 0.9	1.000
1SWASP J084005.72+190130.7	1090-0167104	4.80	0.649	10.00	12.5	0.7	-38.0 ± 6.3, -15.2 ± 6.4	0.960
1SWASP J084022.41+203827.1	1106-0171109	14.59	0.865	11.22	14.3	1.0	-38.0 ± 1.0, -14.0 ± 2.0	1.000
1SWASP J084025.56+192832.8	1094-0163661	13.15	0.241	8.76	9.7	0.2	-36.7 ± 0.8, -13.3 ± 0.7	0.999
1SWASP J084033.46+193801.0	1096-0164636	9.34	0.537	10.16	12.3	0.1	-41.1 ± 6.3, -13.9 ± 6.4	0.999
1SWASP J084036.23+213342.1	1115-0176177	$8.88^{0.119}$	0.421	9.97	11.8	1.9	-36.8 ± 1.1, -14.2 ± 0.6	0.995
1SWASP J084044.25+202818.7	1104-0163841	4.27	0.839	10.40	13.8	0.8	-36.0 ± 4.0, -10.0 ± 4.0	0.906
1SWASP J084047.61+185411.9	1089-0167723	8.89	0.440	9.68	11.2	0.8	-36.2 ± 1.2, -14.9 ± 1.2	0.996
1SWASP J084048.34+195518.9	1099-0165066	7.43	0.357	9.50	11.0	0.3	-35.5 ± 1.2, -13.0 ± 0.6	1.000
1SWASP J084055.31+183459.0	1085-0167929	12.49	0.796	11.12	14.0	1.1	-41.2 ± 6.4, -14.2 ± 6.3	0.998
1SWASP J084059.70+182204.5	1083-0186951	9.13	0.578	9.68	11.5	1.3	-41.4 ± 5.2, -12.5 ± 5.7	0.995
1SWASP J084122.57+185602.0	1089-0167811	11.16	0.626	10.53	12.9	0.8	-35.4 ± 6.3, -11.2 ± 6.4	0.994
1SWASP J084130.69+185218.6	1088-0167362	2.43	0.616	10.15	12.7	0.9	-36.0 ± 2.0, -12.0 ± 3.0	0.999
1SWASP J084143.67+195743.8	1099-0165295	9.15	0.507	10.25	12.4	0.4	-40.5 ± 1.9, -13.1 ± 1.9	0.989
1SWASP J084158.83+200627.2	1101-0162974	11.08	0.644	10.59	13.0	0.6	-44.1 ± 6.3, -18.1 ± 6.3	0.999
1SWASP J084220.09+190905.7	1091-0165816	12.04	0.698	10.69	13.2	0.7	-37.0 ± 6.3, -16.8 ± 6.5	0.998
1SWASP J084237.01+200832.0	1101-0163099	12.22	0.763	10.87	13.7	0.7	-42.4 ± 6.4, -16.5 ± 6.4	1.000
1SWASP J084245.96+211616.3	1112-0175801	$3.52^{0.001}$	0.811	10.92	14.0	1.7	-36.0 ± 3.0, -12.0 ± 1.0	1.000
1SWASP J084248.47+203424.5	1105-0167705	9.95	0.531	10.26	12.4	1.1	-35.2 ± 2.0, -13.1 ± 2.0	1.000
1SWASP J084308.22+194247.7	1097-0164856	11.71	0.631	10.66	13.1	0.6	-43.9 ± 6.3, -17.8 ± 6.3	0.998
1SWASP J084317.83+203037.3	1105-0167843	8.91	0.542	9.77	12.0	1.1	-37.3 ± 1.3, -14.2 ± 2.0	0.981
1SWASP J084332.39+194437.8	1097-0164949	9.75	0.537	10.21	12.3	0.7	-40.0 ± 2.0, -16.5 ± 2.0	0.961
1SWASP J084344.72+211234.5	1112-0175989	$2.83^{0.004}$	0.836	11.41	14.8	1.7	-38.0 ± 2.0, -12.0 ± 3.0	1.000
1SWASP J084519.17+190010.9	1090-0168262	12.30	0.758	10.89	13.5	1.3	-43.9 ± 6.3, -11.5 ± 6.3	0.997
1SWASP J084624.31+170235.1	1070-0184311	11.43	0.674	10.19	12.9	3.0	-51.8 ± 6.0, -8.5 ± 6.0	0.945
1SWASP J084647.32+193840.9	1096-0165969	6.28	0.279	9.34	10.9	1.5	-36.5 ± 0.6, -13.9 ± 1.0	1.000
1SWASP J084714.12+162347.3	1063-0162881	5.70	0.267	9.29	10.6	3.7	-37.7 ± 1.2, -12.6 ± 1.3	1.000
1SWASP J084817.25+165447.7	1069-0177337	11.25	0.739	10.59	13.5	3.3	-42.7 ± 6.0, -18.8 ± 6.1	1.000
1SWASP J084847.83+274136.5	1176-0212100	12.36	0.780	10.58	13.7	8.2	-52.5 ± 5.2, -18.8 ± 5.2	0.994
1SWASP J084948.35+160750.7	1061-0165009	11.38	0.503	10.43	12.6	4.2	-44.8 ± 6.0, -11.6 ± 6.0	0.997
1SWASP J090222.37+182223.9	1083-0190841	14.82	0.611	10.34	12.6	5.4	-32.0 ± 2.0, -8.0 ± 3.0	0.671

the period–colour relation but that the period analysis found the half-period harmonic. This phenomenon, already observed in the Hyades for 1SWASP J044735.33+145320.7 and in Coma (see CC09), is relatively common and is caused by diametrally symmetric stellar spot patterns. Among the other outliers, 1SWASP J090222.37+182223.9 has a relatively low membership probability (67 per cent) and 1SWASP J084025.56+192832.8 stands out in the colour–magnitude diagram (Fig. 5) as a likely binary, which can affect its period or colour. The fast rotator 1SWASP J084130.69+185218.6 with $J - K_s = 0.616$ seems a regular object and is difficult to explain. It could however be a contrasted tidally locked binary, but we have no way to ascertain this for now.

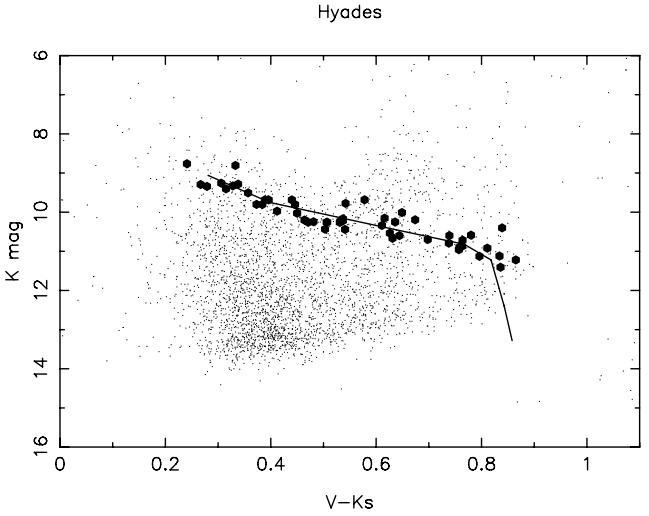

Figure 12. Colour–magnitude diagram of field stars (dots) and Praesepe selected members (black circles). The Praesepe main sequence is shown as a black line.

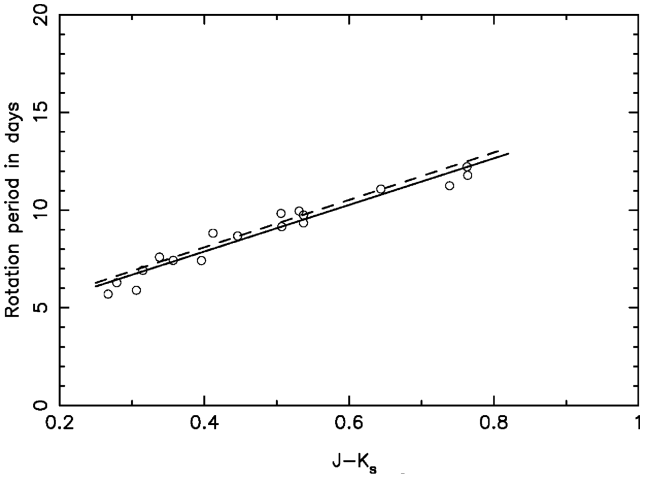

Figure 13. Colour–period diagram and relation of a biased Praesepe sample obtained by manually setting a very tight constraint (sigma of 0.075 mag) on the colour–magnitude selection. Black line is the resulting colour–period relation. The regular colour–period relation obtained with the full sample is shown a dashed line for comparison.

Fig. 14 shows the cluster members retained to derive the following colour–period relation:

$$P = 9.648 + 12.124(J - K_s - 0.528).$$

The standard deviation around the relation is 0.46 d, again much higher than the measurement error on periods which is between 0.1 and 0.2 d. It seems that for Praesepe as much as for the Hyades, the period–colour relation has not perfectly converged yet and is still slightly dependent on the initial condition at the formation of the cluster. However, it should be again remarked that the scatter derived for the Coma cluster by CC09 is only 0.19 d, while the cluster has about the same age as Praesepe and the Hyades. This could be a selection bias on CC09 Coma cluster member selection. Indeed Coma proper motion locus is within 1σ of the field proper motion distribution, and since the dispersion of the field proper motion is much larger than the dispersion of the cluster proper motions, objects close to both loci will systematically be classified as field objects rather than cluster members, unless the object's colour is close enough to the cluster main sequence to push the cluster membership probability over our $p > 0.5$ threshold. This biased the Coma sample towards keeping only members which are very close to the cluster proper motion and colour loci, resulting in less contamination and significant loss of completeness. Our study of Hyades and Praesepe uses the same cluster membership rationale but does not suffer from this bias because these cluster's proper motion locus is very far from the proper motion distribution of the field. We created a similar bias in Praesepe by manually setting the sigma of the colour–magnitude distribution in the cluster membership calculation routines to a very small value (0.075 mag) and obtained a similarly tight colour–period relation on the smaller number of candidates selected (see Fig. 13) with a scatter of 0.23. The number and dispersion of the selected objects is very similar to what is observed for Coma by CC09. Note that the same procedure is not applicable to the Hyades because of the natural spread in magnitudes (see Fig. 5) induced by the large spatial extent of the cluster.

The astrophysical relation between selecting objects closer to the main sequence at a given age and obtaining a tighter colour–period relation is not obvious and is likely down to a combination of several possible causes such as the following.

(i) Selecting only objects with magnitudes very close to the expected main sequence removes most of low to moderate contrast binaries. This eliminates the effect of unresolved binarity on periods and also colours that can increase the period–colour scatter.

(ii) Objects whose colour or magnitude is affected by photometric measurement errors of any cause would be excluded. This directly removes most of the scatter in the period–colour relation which is due to colour measurement error.

(iii) Any object showing a noticeable colour or apparent magnitude variation from the main sequence due to a higher or a lower than average spot coverage would be excluded from the member list. Since there is a strong correlation between rotation period and spot coverage, this could also tend to select only objects with more average colour and rotation.

(iv) If there is any actual age spread within a cluster, a tighter colour–magnitude selection would eliminate older or younger objects, thus removing any scatter in the period–colour relation that could arise from age variations.

(v) More generally, the colour–period relation actually stems from a mass–period relation. Any factor such as metallicity or individual star history, which would affect the colour–mass–magnitude relation would increase the scatter in the period–colour relation and would be cut out by tighter constraints on the colour–magnitude selection.

6 COMPARISON BETWEEN THE HYADES AND PRAESEPE: AGE AND BRAKING

6.1 Braking time-scales

Deriving stellar rotation braking time-scales over a wide range of stellar masses, and especially in the M-dwarf regime where stars become entirely convective, puts strong constraints on theoretical models of magnetic field/rotational braking. As seen in Figs 6 and 14, our survey determined rotation periods of M-dwarf stars both in the Hyades and Praesepe. However, these figures use the $J - K_s$ colour that tends to saturate for the reddest stars ($J - K_s$ only varies from 0.82 to 0.86 when the stellar mass varies from 0.6 to 0.25 $M_\odot$) that are the most interesting to explore rotational braking

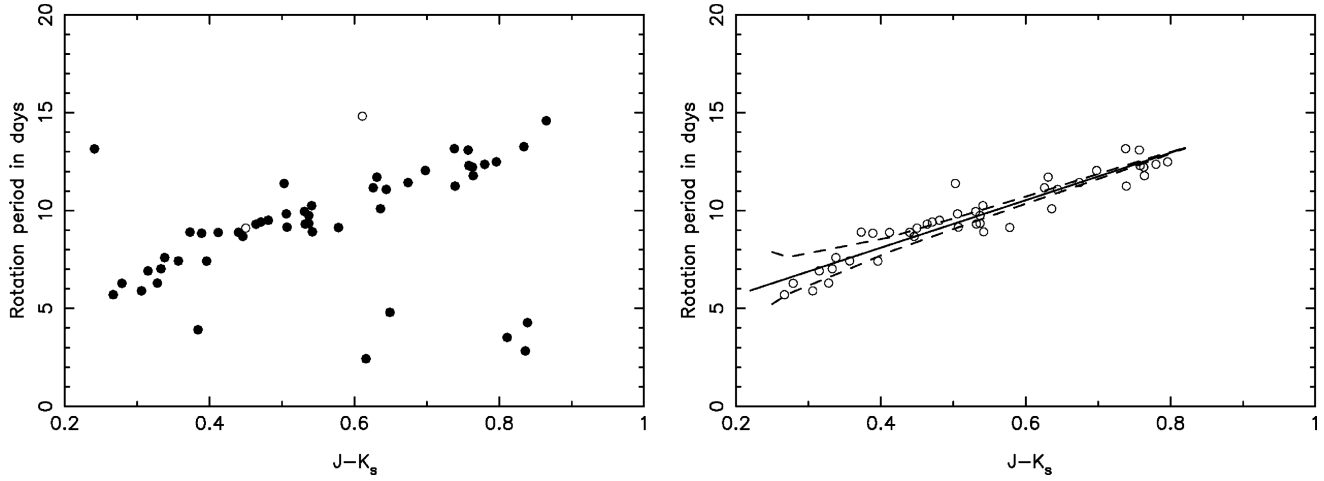

Figure 14. Left: $J - K_s$ colour–period plot of all selected Praesepe members. Right: $J - K_s$ colour–period plot of Praesepe members that are used to derive the colour–period relation (black line). The corresponding masses at 600Myr (in $M_\odot$) are given below the colour scales.

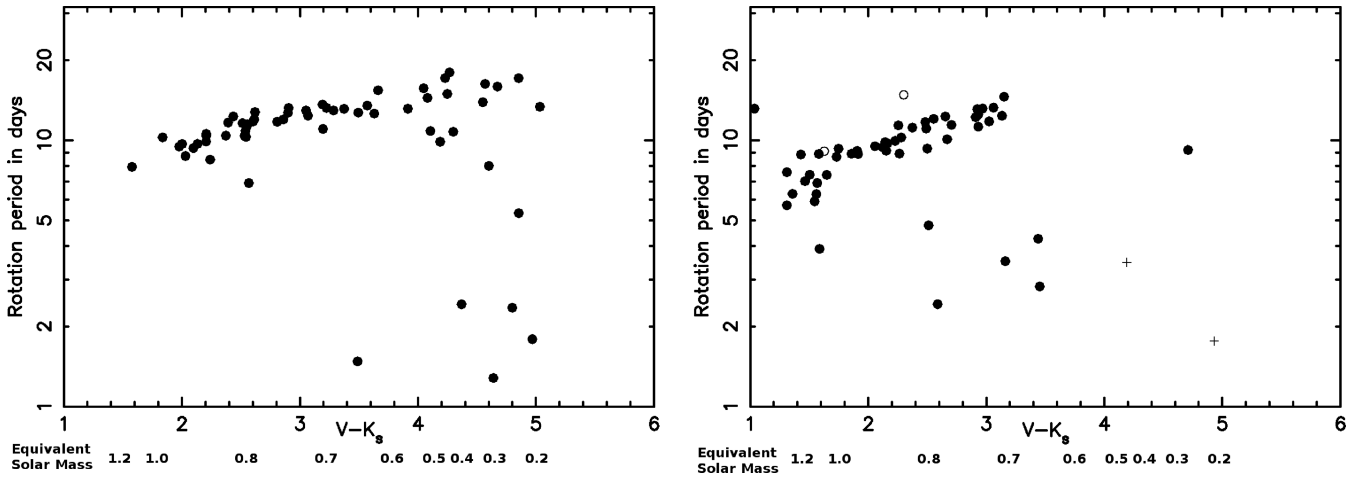

Figure 15. Left: log of rotation period–$(V - K_s)$ colour plot of objects identified as Hyades members. Right: same for Praesepe members. The crosses are two Praesepe objects from Scholz & Eislöffel (2007). Full circles are objects with a membership probability above 0.85, hollow circles are objects with a membership probability above 0.5.

time-scales. Fig. 15 shows the logarithmic rotation period as a function of the $V - K_s$ colour which varies from 3.7 to 4.8 as the stellar mass varies from 0.6 to 0.25 $M_\odot$. Given this more than 40 times better colour dynamic for low-mass objects, using the $V - K_s$ colour allows a much more accurate determination of the stellar mass range where the tight colour–period relation breaks down. However, a few of the stars visible in the $J - K_s$ plots do not appear here, because they have no V-band magnitudes. Also, errors on V-band magnitudes are much bigger than error on infrared magnitudes, especially since most of the optical magnitudes are taken from photographic plates.

For the Hyades, this breakdown is obvious because we have a good sampling at low masses: the cluster is nearby and its M dwarfs are bright enough to derive reliable rotation periods. It seems to occur for $V - K_s > 4.0$ (i.e. masses $\sim <0.5\,M_\odot$), with the apparition of numerous fast rotators as well as a significant increase of the slow rotators scattering around the colour–period relation. However, several slow rotators with periods in good agreement with the colour–period relation are still observed down to the lowest masses sampled by our survey, around 0.2 $M_\odot$. The Hyades data therefore demonstrate that FGK and M stars above 0.5 $M_\odot$ have converged towards a simple colour–period relation by Hyades age, about 625 Myr.

The breakdown of the period–colour relation is less clear cut for Praesepe because this cluster is farther away and the survey detection limit is in the late K/early M-dwarf range. It is however clear that objects bluer than $V - K_s = 3.2$ (or above 0.65 $M_\odot$) have converged towards the colour–period relation by Praesepe age. Three fast rotators (1SWASP J084044.25+202818.7, 1SWASP J084245.96+211616.3 and 1SWASP J084344.72+211234.5, the two latter being independently identified during two seasons at the same period) are however detected for $V - K_s = 3.1$–3.4, respectively 3.4, 3.1 and 3.4. This corresponds to a mass of $\sim$0.65 $M_\odot$ in the late K-dwarf range, where just one Hyades fast rotator (a spectroscopic binary) is identified. However, the V magnitude of these faint red Praesepe members is not very accurate, and they are possibly later type objects, as hinted by their $J - K_s$ colours, 0.839, 0.811 and 0.836 which would put all but one in the M-dwarf range. Spectroscopy from Allen & Strom (1995) gives spectral types of K6, K7.5 and M0.8, which would put the last one, 1SWASP J084344.72+211234.5, outside the mass range where other Praesepe members have converged towards a clean colour–period

relation. This leaves 1SWASP J084044.25+202818.7 and 1SWASP J084245.96+211616.3 as unexpected fast-rotating Praesepe members.

If these two objects are representative of the actual late K-dwarf cluster population, that would mean that Praesepe is significantly younger than the Hyades, even more than the 50 Myr we derive in the next section. Indeed, since all objects observed in this mass range in the Hyades have spun down to 11–13 d period, the age difference between the two clusters must be significant enough to allow these Praesepe fast rotators to spin-down from their current 3.5–5 d period to 11–13 d when they will be of Hyades age.

Assuming a naive constant braking rate would have these objects rotating well beyond their break-up velocities when they were 300-Myr old or younger. Since the braking rate is supposed to decrease with time, it is even more incompatible with wind-driven angular momentum loss in just 50 Myr. However, an age difference significantly larger than that would be surprising because Praesepe and the Hyades have been found to be of similar age.

The alternative is that these two late K Praesepe fast rotators would be short-period binaries (<12 d according to Meibom & Mathieu 2005; Mazeh 2008; Raghavan et al. 2010), which are not expected to follow the colour–period relation because of tidal interactions. A few per cent of solar-type stars are expected to be short-period binaries (Abt & Levy 1976; Duquennoy & Mayor 1991), making plausible that these Praesepe fast rotators are such. They are not known as short-period binaries, but they have not surveyed for this. 1SWASP J084044.25+202818.7 appears significantly overluminous in a colour–magnitude diagram and at least this one is likely an equal mass binary. It is therefore possible that both of them are close binaries and would be simpler to account than a major age difference between the two clusters, but this would need to be confirmed.

Scholz & Eislöffel (2007) have probed the mid-/late M-dwarf rotation periods in Praesepe and found only fast rotators. We added the two objects from their study which have *V*-band NOMAD magnitudes (the most massive of the five they studied) in Fig. 15. Together with our SWASP data, this shows that Praesepe stars rotation rate have clearly converged for masses higher than 0.65 $M_\odot$ and have not converged in the mid-/late M-dwarf range. The colour–period relation breakdown in Praesepe must then occur in between 0.65 and 0.4 $M_\odot$ mass range. The picture is still unclear in this range because there is no significant overlap between Scholz & Eislöffel (2007) and our survey. A more accurate determination of the colour–period relation in Praesepe would need more data on early M-dwarfs rotation periods in the cluster and/or to ascertain whether or not the three red fast rotators we identified are spectroscopic binaries.

6.2 Gyrochronological ages of the Hyades and Praesepe

Barnes (2003) coined the word 'gyrochronology' to describe the technique that permits us to derive the age of a star when its rotation period is known. This assumes, following the early study of Skumanich (1972), that the rotation period of stars of given mass converges after a certain time to the same value independently of the initial conditions and that their rotation period then evolves following a simple spin-down law where $P \propto t^b$, with $b = 0.5$ defined as the magnetic braking index. The data presented here confirm that Hyades and Praesepe stars with $0.2 < J - K_s < 0.82$ have already converged towards a well-defined colour–rotation period relation.

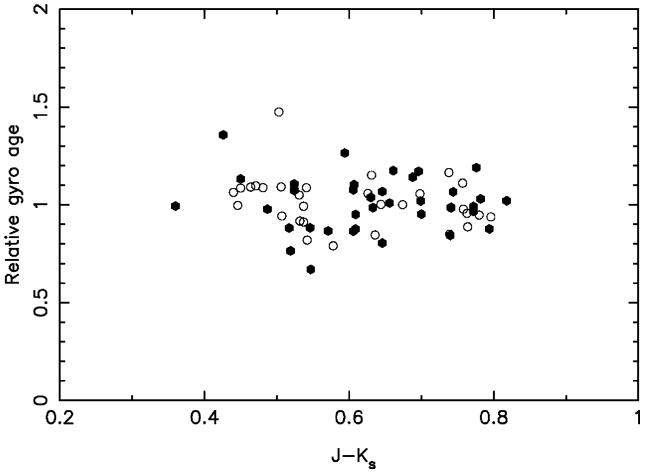

Figure 16. Relative age of individual Hyades members (black circles) and Praesepe members (hollow circle) for slow rotators with $0.2 < J - K_s < 0.82$, assuming an arbitrary age of one for both clusters.

6.2.1 *Intracluster age distribution*

Any star in this colour range can have its period, and thus its age, compared to the average period of the clusters, as defined by the colour–period relation of each cluster. We can therefore use their rotation periods to accurately compute the relative age distribution within each cluster. The age of an individual star relative to the fiducial rotational age $t_{\rm cluster}$ of the each population is given by

$$t = t_{\rm Hyades}\left[\frac{P}{11.401 + 12.652(J - K_s - 0.631)}\right]^2, \quad (7)$$

$$t = t_{\rm Praesepe}\left[\frac{P}{9.648 + 12.124(J - K_s - 0.528)}\right]^2. \quad (8)$$

Setting the cluster ages to the arbitrary value of 1, we obtain an average age for the Hyades sample of 1.006, with a dispersion of 0.14 and an average of 1.003 for the Praesepe sample, with a dispersion of 0.10 (see Fig. 16). Note that these are relative ages within each cluster which are meant to illustrate the dispersion in age measurements within each cluster (which stems from the dispersion around the period–colour relation and is not necessarily an actual age dispersion) and are not relevant to compare the age of the cluster themselves. Under the assumption that all stars in each cluster have about the same age, the dispersions of 10 and 14 per cent we derive here are representative of the accuracy of gyrochronology to measure the age of individual stars.

6.2.2 *Relative age of Praesepe compared to the Hyades*

To derive Praesepe's age relatively to the Hyades, we anchored the age–period relation assuming a mean Hyades age of 625 Myr (P98). We derived the age of Praesepe stars by computing the rotation period they would have if they had the age of Hyades and comparing this hypothetical period to the measured one we were able to compute an age for each slow rotator with $0.2 < J - K_s < 0.82$ in Praesepe as follows:

$$t = 625\left[\frac{P}{11.401 + 12.652(J - K - 0.631)}\right]^2. \quad (9)$$

The age of Praesepe was derived from the averaged ages of these 43 stars, and stands at 573 ± 13 Myr. We carried out the same

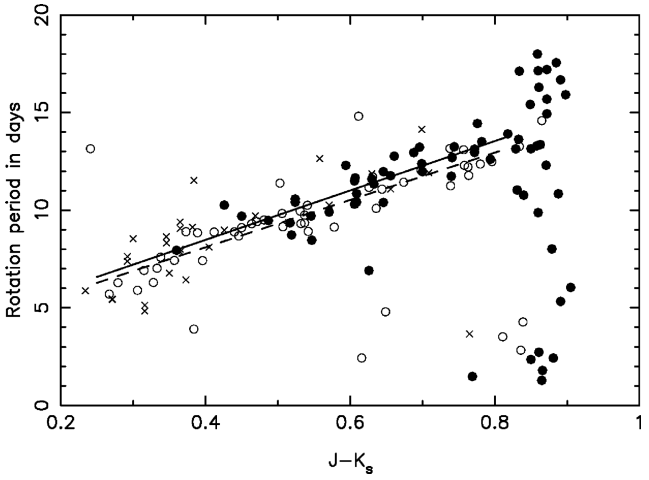

Figure 17. $J - K_s$ colour–period plot of Hyades (black circles for SWASP objects and crosses for R87–95 objects) and Praesepe members (hollow circle). The period–colour relation are also shown, black line for the Hyades and dashed line for Praesepe.

analysis for the Hyades. The average age of the stars in the Hyades sample is 628 ± 14 Myr. These absolute values need to be taken with caution since the uncertainties on the actual Hyades age, that we use to anchor the relation, are much bigger (±50 Myr; Perryman et al. 1998) than our errors. However, the relative measurements are much more reliable and a Student *t*-test on these $0.2 < J - K_s < 0.82$ samples showed that there is only 1.5 per cent likelihood they derive from the same age distribution. This means it is highly probable that Praesepe is actually younger than the Hyades, our results pointing towards a 50-Myr age difference. These quantitative results are backed by the qualitative appearance of the clusters' colour–period plots, Praesepe stars having shorter periods in average (see Fig. 17). As seen in the previous section, this might also be supported by the presence of bluer fast rotators in Praesepe than in the Hyades.

Using our new SWASP data for the Hyades and CC09 data for the Coma cluster, we also derived an improved estimation of Coma's age: 580 ± 12 Myr. This agrees well with the 591 ± 41 Myr found by CC09 using older Hyades data (from R87–95) to calibrate the cluster's age and puts Coma almost exactly at the same age as Praesepe. The ages derived with the improved gyrochronological relation described in the last section of this article are quite similar, with an age of 578 ± 12 Myr for Praesepe and 584 ± 10 Myr for Coma.

6.2.3 Individual stars age distribution relative to Hyades age

Fig. 18 shows the ages of individual stars in our sample for each of these three clusters. The large scatter in ages observed on this figure is likely not real but most of it is probably due to the scatter of the colour–period–age relation at about 600 Myr. This scatter is 85 Myr for the Hyades, 85 Myr for Praesepe and 61 Myr for Coma (respectively 76, 77 and 55 Myr with the improved gyrochronological relation), showing that at these ages the simple gyrochronology spin-down law from Skumanich (1972) enables age measurements for individual stars with a better than 15 per cent accuracy, improving as the square root of the number of cluster members when measuring the age of a cluster. If this relation is properly calibrated for field stars, gyrochronology should provide even more accurate age measurements for individual field stars because the scatter of the colour–period–age relation is expected to decrease with age.

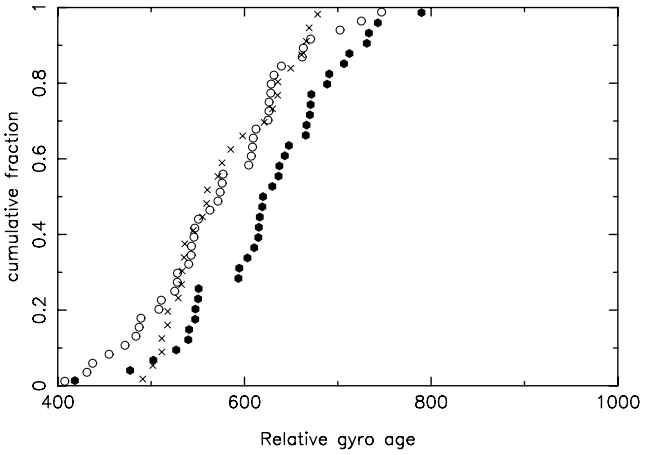

Figure 18. Cumulative fraction plot of Hyades members ages (black circles), Praesepe members ages (hollow circles) and Coma members ages (crosses).

This excellent precision in relative age measurement would be extremely valuable even if it is somewhat degraded by systematic errors arising from calibration of the technique.

7 CALIBRATION OF GYROCHRONOLGY: THE AGE OF FIELD STARS

7.1 Combining all SWASP cluster data into an homogeneous set

In order to calibrate gyrochronology using all the SWASP clusters data, we numerically aged the rotation periods of Praesepe and Coma stars from CC09 up to the Hyades age of 625 Myr. We assumed a Skumanich braking law to derive this $P_{\rm Hyades}$:

$$P_{\rm Hyades} = P_{\rm Cluster}\left(\frac{\rm Age_{Hyades}}{\rm Age_{Cluster}}\right)^{1/2}.$$

We then fitted a simple linear relation through this combined data set of all 109 cluster stars with SWASP periods, in the same way we obtained the individual cluster period–colour relation. This gave the following period–colour relation that we used to derive the age of field stars:

$$P = 10.603 + 12.314(J - K_s - 0.570).$$

The resulting dispersion around the relation is 0.45 d. This compares remarkably well with the weighted average of the dispersion around the three clusters colour–period relation, which stands at 0.44 d: the artificial 'ageing' of the rotation periods introduces almost no noise in the combined data. Fig. 19 shows the periods and colour of stars in this combined cluster data set and the relation fitted through.

7.2 The age of field stars: comparison with asteroseismology

The period–colour relation from the combined SWASP cluster data set gives us a statistically robust estimates of the rotation of FGK and early M stars by Hyades ages. We can derive the age of the Sun given its rotation period using the following relation:

$$\rm Age_{Sun} = Age_{cluster}\left[\frac{Period(Sun)}{Period(1\,M_\odot\ star\ in\ cluster)}\right]^2. \quad (10)$$

Using the isochrones from Pinsonneault et al. (2004), we have $J - K_s = 0.399$ for a $1\,M_\odot$ star in the Hyades, which translates

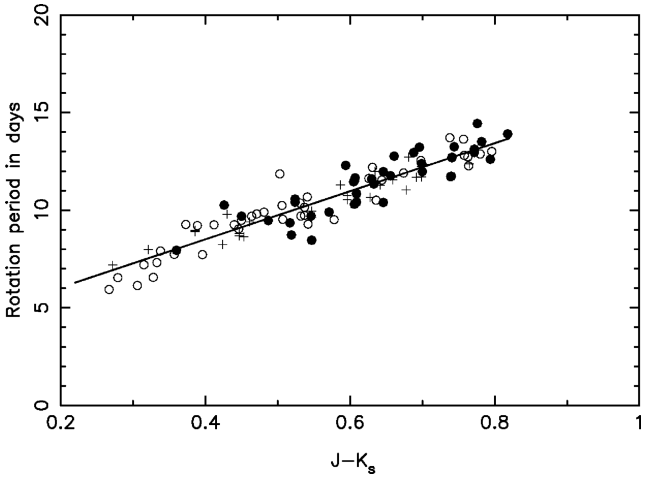

Figure 19. Period–colour relation for Hyades members ages (black circles), artificially aged Praesepe members ages (hollow circles) and artificially aged Coma members ages (crosses).

into a period of 8.5 d at Hyades ages. Assuming the Hyades ages is 625 Myr, neglecting any metallicity effect, this relation with no further calibration gives the Sun an age of 5870 ± 630 Myr, 2σ or about 30 per cent away from its measured age of 4570 Myr (5). The error stated here comes from the dispersion around the colour–period relation and assumes the rotation period of the Sun at the mid-latitude sunspot belt is 26.1 d (Donahue, Saar & Baliunas 1996) and has no errors. The same calculation can be applied to any star with an accurate age measurement and a known rotation period. Following CC09, we determine the gyrochronological ages of the only three stars in the FGKM spectral range with accurate age determination from asteroseismology assuming there is no systematic error in these ages derived from asteroseismology.

Their $J - K$ colours at Hyades ages were determined using the masses of the stars and the Pinsonneault et al. (2004) isochrones. The mass of αCenA was taken as 1.1 $M_\odot$ and αCenB as 0.91 $M_\odot$ following Pourbaix, Neuforge-Verheecke & Noels (1999) and the mass of 70OphA as 0.89 $M_\odot$, from Eggenberger et al. (2008). The rotation periods are from Donahue et al. (1996) for the Sun, Barnes (2007) for α Cen, and from Stimets & Giles (1980) and Noyes et al. (1984) for 70 Oph A. The last row is based on the supposition that the true period of 70 Oph A is twice the measured period, which may be a higher frequency harmonic of the true period, as we observed for some cluster stars. The asteroseismological ages for α Cen and 70 Oph A are from Eggenberger et al. (2004, 2008). With the exception of the Sun, the main source of error is the uncertainty on the stars' periods. The results using the standard magnetic braking index $b = 0.5$ are shown in the fourth column of Table 5. The ages found are systematically older than the asteroseismological ages or the age of the sun, and are about 30 per cent off, which is already as good or even better than most of the age measurement methods currently available.

Since the Skumanich (1972) square root braking law derives from a simple magnetic field/angular momentum coupling models, it is expected that some of the parameters it neglects, such as for instance the evolution of the momentum of inertia of a star as it ages, could slightly modify this power law. We therefore calibrated the gyrochronology relation by assuming a slightly different magnetic braking index, $b = 0.56$, already used by CC09. Using this modified law, the period–colour relation we derived from the combined SWASP cluster data set gives an almost exact age for the Sun, of 4.6 ± 0.4 Gyr. The resulting ages for the others stars are shown in the fifth column of Table 5 and are also much closer to the asteroseismological ages than those derived from the standard braking law. Note that assuming $b = 0.56$ instead of 0.5 does not noticeably affect the artificial ageing of Coma and Praesepe described above because these clusters have very similar ages.

Another way to calibrate gyrochronology without modifying the magnetic braking index would be to assume that the Hyades are younger than 625 Myr. However, we would need to assume that the Hyades are much younger, 525-Myr old, to obtain a solar age of 4.9 ± 0.5 Gyr, and this would still not fit the other stars asteroseismological ages within 1σ.

We therefore conclude that calibrating gyrochronology by assuming a modified magnetic braking index with $b = 0.56$ provides a much better fit of the ages of the sample of stars considered here. Given the small age difference between Coma, Praesepe and the Hyades, this new calibration induces a less than 1 per cent difference in their relative age. The corresponding ages are 578 ± 12 Myr for Praesepe and 584 ± 10 Myr for Coma.

Barnes (2007) already demonstrated that gyrochronology produced much more self-consistent age measurements than chromospheric activity and isochrone fitting. When period measurement is accurate (which is only the case of the Sun in Table 5), we have shown in Sections 6.2.1 and 6.2.2 that our age measurements by gyrochronology for individual stars have an accuracy of 10–15 per cent. Our results therefore confirm earlier forecasts by CC09, Barnes (2007) and Mamajek & Hillenbrand (2008) that correctly calibrated gyrochronological ages could give absolute age measurements with an accuracy of around 10 per cent for field stars in the FGK and early M spectral range. Note that this age–rotation period cannot be applied to derive a quantitative measurement of the age of stars younger than their magnetic braking convergence time, shown here to be ∼600 Myrs for late K and early M-dwarfs. Hotter stars converge earlier, and F and G dwarfs have converged towards a clean colour–period relation at the age of M35 (150 Myr; Meibom et al. 2009). Achieving this accuracy would only necessitate measuring the period of the star with an accuracy comparable to SWASP's. However, these results need to be confirmed by

Table 5. Gyrochronological ages for the Sun and old main-sequence stars with measured rotation periods and asteroseismological age determinations.

Star	$J - K$ at Hyades age	Period (d)	GyroAge ($b = 0.5$)	GyroAge ($b = 0.56$)	Seismo Age(Gyr)
Sun	0.399	26.1 ± 0.0	5.9 ± 0.6	4.6 ± 0.4	4.57
αCenA	0.33	28.0 ± 3.0	8.5 ± 2.1	6.4 ± 1.4	6.5 ± 0.3
αCenB	0.49	36.9 ± 1.8	9.2 ± 1.2	6.9 ± 0.8	6.5 ± 0.3
70OphA	0.51	19.9 ± 0.5	2.5 ± 0.3	2.2 ± 0.2	6.2 ± 1.0
70OphA	0.51	39.8 ± 1.0	10.2 ± 1.1	7.5 ± 0.7	6.2 ± 1.0

comparing with a larger sample of stars with independent and accurate age measurements. To our knowledge there are no such objects beyond those discussed here.

8 CONCLUSION

We presented an analysis of SWASP data that found more than 120 rotational variables that we identified as Hyades and Praesepe cluster members. This allowed us to put strong constraints on the rotational braking time by showing that the periods of all FGK and M single stars down to $\sim 0.5\,M_{\odot}$ in our sample have converged towards a relatively tight period–colour relation by Hyades age. We used gyrochronological relations and the period–colour relations derived for each cluster to accurately measure their relative ages, assuming the Hyades are 625-Myr old. This yields ages of 578 ± 12 Myr for Praesepe and 584 ± 10 Myr for Coma and gives a statistically strong statement that Praesepe and the Hyades are not exactly coeval and that the former is 47 ± 17 Myr younger than the latter. We finally used the combined SWASP data using the Hyades stars, and artificially aged Praesepe and Coma stars to derive a global period–colour relation at Hyades age. We used it to calibrate the gyrochronology age relation with a modified magnetic braking index that fits well the age of the Sun and of the few stars with accurate asteroseismological ages. This relation already gives reliable ages and hints that when properly calibrated, gyrochronology could be used to measure the absolute age for any FGK and early-M single field stars with an accuracy of about 10 per cent, provided their rotation period is measured.

ACKNOWLEDGMENTS

The WASP consortium consists of representatives from the Universities of Keele, Leicester, the Open University, Queens University Belfast and St Andrews, along with the Isaac Newton Group (La Palma) and the Instituto de Astrofisica de Canarias (Tenerife). The SuperWASP and WASP-S cameras were constructed and operated with funds made available from Consortium Universities and PPARC/STFC. This publication makes use of data products from the Two Micron All Sky Survey, which is a joint project of the University of Massachusetts and the Infrared Processing and Analysis Censer/California Institute of Technology, funded by the National Aeronautics and Space Administration and the National Science Foundation. This research has made use of the VizieR catalogue access tool, CDS, Strasbourg, France.

REFERENCES

Abt H. A., Levy S. G., 1976, ApJS, 30, 273
Allen L. E., Strom K. M., 1995, AJ, 109, 1379
Barnes S. A., 2003, ApJ, 586, 464
Barnes S. A., 2005, BAAS, 37, 488
Barnes S. A., 2007, ApJ, 669, 1167
Bouvier J., Forestini M., Allain S., 1997, A&A, 326, 1023
Collier Cameron A., Jianke L., 1994, MNRAS, 269, 1099
Collier Cameron A., Campbell C. G., Quaintrell H., 1995, A&A, 298, 133
Collier Cameron A. et al., 2006, MNRAS, 373, 799
Collier Cameron A. et al., 2009, MNRAS, 400, 451 (CC09)
Donahue R. A., Saar S. H., Baliunas S. L., 1996, ApJ, 466, 384
Duquennoy A., Mayor M., 1991, A&A, 248, 485
Edelson R. A., Krolik J. H., 1988, ApJ, 333, 646
Eggenberger P., Charbonnel C., Talon S. et al., 2004, A&A, 417, 235
Eggenberger P., Miglio A., Carrier F., Fernandes J., Santos N. C., 2008, A&A, 482, 631
Girard T., Heisler C., Lee Y. W., López C. E., van Altena W. F., Ianna P. A., 1989, BAAS, 21, 1106
Hartman J. D. et al., 2009, ApJ, 691, 342
Hartman J. D., Bakos G. Á., Kovács G., Noyes R. W., 2010, MNRAS, 408, 475
Irwin J., Bouvier J., 2009, in Mamajek E. E., Soderblom D. R., Wyse R. F. G., eds, IAU Symp. Vol. 258, The Ages of Stars. Cambridge Univ. Press, Cambridge, p. 363
James D. J. et al., 2010, A&A, 515, 100
Johnson H. L., 1952, ApJ, 116, 640
Jones B. F., Stauffer J. R., 1991, AJ, 102, 1080
Kawaler S. D., 1988, ApJ, 333, 236
Klein Wassink W. J., 1927, Publ. Kapteyn Astron. Lab. Groningen, 41, 1
Kraft R. P., 1967, ApJ, 150, 551
Kraus A. L., Hillenbrand L. A., 2007, AJ, 134, 2340
Loktin A. V., Beshenov G. V., 2003, Astron. Rep., 47, 6
Mamajek E. E., Hillenbrand L. A., 2008, ApJ, 687, 1264
Mazeh T., 2008, in Goupil M.-J., Zahn J.-P., eds, EAS Publ. Ser. Vol. 29, Observational Evidence for Tidal Interaction in Close Binary Systems. EDP Sciences, Paris, p. 1
Meibom S., Mathieu R. D., 2005, ApJ, 620, 970
Meibom S., Mathieu R. D., Stassun K. G., 2009, ApJ, 695, 679
Mermilliod J., Weis E. W., Duquennoy A., Mayor M., 1990, A&A, 235, 114
Mermilliod J., Mayor M., Udry S., 2009, A&A, 498, 949
Noyes R. W., Hartmann L. W., Baliunas S. L., Duncan D. K., Vaughan A. H., 1984, ApJ, 279, 763
Perryman M. A. C., 1998, A&A, 331, 81 (P98)
Pinsonneault M. H., Terndrup D. M., Hanson R. B., Stauffer J. R., 2004, ApJ, 600, 946
Pollacco D., 2006, Ap&SS, 304, 253
Pourbaix D., Neuforge-Verheecke C., Noels A., 1999, A&A, 344, 172
Radick R. R., Thompson D. T., Lockwood G. W., Duncan D. K., Baggett W. E., 1987, ApJ, 321, 459
Radick R. R., Lockwood G. W., Skiff B. A., Thompson D. T., 1995, ApJ, 452, 332
Raghavan D. et al., 2010, ApJS, 190, 1
Reid N., 1992, MNRAS, 257, 257
Reiners A., 2006, A&A, 446, 267
Scholz A., Eislöffel J., 2007, MNRAS, 381, 1638
Skumanich A., 1972, ApJ, 171, 565
Stauffer J., 1982, AJ, 87, 899
Stern R. A., Schmitt J. H. M. M., Kahabka P. T., 1995, ApJ, 448, 683
Stimets R. W., Giles R. H., 1980, ApJ, 242, L37
Sukhbold T., Howell S. B., 2009, PASP, 121, 1188
Tamuz O., Mazeh T., Zucker S., 2005, MNRAS, 356, 1466
Upgren A. R., Weis E. W., Deluca E. E., 1979, AJ, 84, 1586
Upgren A. R., Weis E. W., Hanson R. B., 1985, AJ, 90, 2039
van Leeuwen F., 2009, A&A, 497, 209
Weber E. J., Davis L., Jr, 1967, ApJ, 148, 217
Weis E. W., 1981, PASP, 93, 437
Weis E. W., 1983, PASP, 95, 29
Weis E. W., Hanson R. B., 1988, AJ, 96, 148
Zechmeister M., Kürster M., 2009, A&A, 496, 577

APPENDIX A: GAS-IDENTIFICATIONS WITH KNOWN CLUSTER MEMBERS

Table A1. Cross-identifications and *B*, *V* photometry from the literature of rotational variables with Hyades membership probabilities greater than 0.5. The 1SWASP identifier encodes the J2000.0 coordinates of the object.

1SWASP	USNO B-1.0	Cluster member ID	Spectral type	*V*	*B* − *V*	Reference
1SWASPJ033734.97+212035.4	1113-0041831	Melotte 25 5	G5	9.36	0.92	2
1SWASPJ034347.07+205136.4	1108-0041451	–	–	14.54	9	4
1SWASPJ035234.31+111538.6	1012-0033507	–	M	13.73	1.54	2
1SWASPJ035453.20+161856.3	1063-0039925	–	M	14.25	1.58	2
1SWASPJ035501.43+122908.1	1024-0045401	Melotte 25 S 155	M0	10.12	1.07	1
1SWASPJ040339.03+192718.1	1094-0044958	Melotte 25 222	K5	10.17	1.08	2
1SWASPJ040525.67+192631.7	1094-0045433	Melotte 25 226	K7	11.41	1.35	1
1SWASPJ040634.62+133256.8	1035-0040066	Melotte 25 REID 62	M	13.52	1.47	9
1SWASPJ040701.22+152006.0	1053-0044486	Melotte 25 231	K5	10.49	1.18	1
1SWASPJ040743.19+163107.6	1065-0042472	Melotte 25 229	K0	9.94	1.02	2
1SWASPJ040811.02+165223.3	1068-0041870	Melotte 25 REID 72	K7	11.52	1.44	1
1SWASPJ040826.66+121130.6	1021-0043331	Melotte 25 233	M0	11.28	1.33	2
1SWASPJ040836.21+234607.0	1137-0048046	Melotte 25 PELS 18	G5	9.44	0.9	1
1SWASPJ041127.64+155931.8	1059-0051230	Melotte 25 HAN 43	M	15.15	1.65	2
1SWASPJ041510.33+142354.5	1043-0041060	Melotte 25 245	K2	11.54	1.38	2
1SWASPJ041633.47+215426.8	1119-0053591	Melotte 25 21	G5	9.14	0.81	2
1SWASPJ041725.14+190147.4	1090-0048172	Melotte 25 251	K5	10.83	1.22	2
1SWASPJ041728.13+145403.9	1049-0042422	Melotte 25 VA 106	M3	14.46	1.55	5
1SWASPJ042322.85+193931.1	1096-0050945	Melotte 25 43	K2	9.4	0.91	2
1SWASPJ042325.28+154547.2	1057-0062216	Melotte 25 173	K0	10.49	1.24	1
1SWASPJ042350.70+091219.5	992-0039564	–	M3	12.89	1.51	1
1SWASPJ042359.13+164317.7	1067-0045253	Melotte 25 260	M0.5	12.55	1.49	3
1SWASPJ042416.93+180010.4	1080-0063868	Melotte 25 174	K5	9.99	1.06	1
1SWASPJ042500.18+165905.8	1069-0045244	Melotte 25 175	K4	10.3	1.03	1
1SWASPJ042514.54+185824.9	1089-0051192	Melotte 25 PELS 40		12.82	1.48	1
1SWASPJ042547.55+180102.2	1080-0064462	Melotte 25 176	K2	9.01	0.94	1
1SWASPJ042642.81+124111.7	1026-0052108	Melotte 25 269	M0	10.48	1.36	2
1SWASPJ042648.25+105215.9	1008-0039886	Melotte 25 271	K5	9.45	1.04	2
1SWASPJ042725.34+141538.3	1042-0043123	Melotte 25 177	K2	10.3	1.08	4
1SWASPJ042747.03+142503.8	1044-0042884	Melotte 25 179	K0	9.49	0.92	3
1SWASPJ042828.78+174145.1	1076-0062237	Melotte 25 VA 486	M1	12.05	1.49	5
1SWASPJ043033.88+144453.1	1047-0044652	Melotte 25 LH 75	M	14.68	1.56	5
1SWASPJ043034.87+154402.3	1057-0063658	Melotte 25 182	K0	8.93	0.84	1
1SWASPJ043152.40+152958.3	1054-0052709	Melotte 25 191	K0	11.04	1.31	1
1SWASPJ043225.66+130647.6	1031-0059808	Melotte 25 288	K0	10.91	1.19	2
1SWASPJ043323.75+235927.0	1139-0053890	Melotte 25 PELS 74	K6	12.62	1.52	1
1SWASPJ043327.00+130243.6	1030-0056878	–	–	13.16	1.57	1
1SWASPJ043337.18+210903.0	1111-0054738	Melotte 25 290	K0	10.7	1.23	2
1SWASPJ043411.14+113328.4	1015-0040520	Melotte 25 294	K4	11.73	1.39	2
1SWASPJ043548.51+131717.0	1032-0063919	Melotte 25 VA 776	M2.5	14.91	1.63	1
1SWASPJ043605.26+154102.4	1056-0061021	Melotte 25 99	K0	9.37	0.87	2
1SWASPJ043950.97+124342.5	1027-0058818	Melotte 25 311	K5	10.06	1.07	2
1SWASPJ044127.81+140434.1	1040-0045181	–	M2.5	–	–	–
1SWASPJ044128.75+120033.7	1020-0044793	–	–	12.88	1.5	4
1SWASPJ044129.67+131316.3	1032-0065593	Melotte 25 316		11.23	1.44	3
1SWASPJ044142.98+082620.0	984-0050517	–	–	–	–	–
1SWASPJ044315.69+170408.7	1070-0053038	Melotte 25 319	K0	9.86	1	2
1SWASPJ044618.79+033810.7	936-0059947	Melotte 25 326	K4.5	10.93	1.27	2
1SWASPJ044630.38+152819.3	1054-0056655	Melotte 25 142	G5	8.3	0.66	2
1SWASPJ044718.51+062711.6	964-0047473	–	K6	11.33	1.42	2
1SWASPJ044800.88+170321.6	1070-0054253	Melotte 25 331		11.12	1.41	4
1SWASPJ044830.61+162319.0	1063-0051391	–	–	12.42	1.47	4
1SWASPJ044842.13+210603.6	1111-0060275	Melotte 25 115	G5	9.06	0.85	2
1SWASPJ044912.98+244810.2	1148-0059776	Melotte 25 117	K3	9.53	1.04	4
1SWASPJ044952.11+060633.6	961-0047586	–	–	14.73	1.63	4
1SWASPJ045000.70+162443.5	1064-0050763	–	K0	10.61	1.16	1
1SWASPJ045102.41+145816.5	1049-0049205	–	M0	–	–	–
1SWASPJ045223.53+185948.9	1089-0058167	Melotte 25 PELS 98	K0	10.29	1.07	1
1SWASPJ045223.86+104309.9	1007-0045668	–	–	–	–	–
1SWASPJ050540.37+062754.6	964-0053308	Melotte 25 151	K2	9.92	0.95	2

Table A1 – *continued*

1SWASP	USNO B-1.0	Cluster member ID	Spectral type	V	$B-V$	Reference
1SWASPJ051109.69+154857.5	1058-0068980	–	K4.5	–	–	–
1SWASPJ051119.30+075432.0	979-0066501	–	K5	–	–	–

References: 1 – Upgren, Weis & Deluca (1979); 2 – Weis (1983); 3 – Upgren, Weis & Hanson (1985); 4 – Weis & Hanson (1988); 5 – Stauffer (1982).

Table A2. Cross-identifications and B, V photometry from the literature of rotational variables with Praesepe membership probabilities greater than 0.5. The 1SWASP identifier encodes the J2000.0 coordinates of the object.

1SWASP	USNO B-1.0	Cluster member ID	Spectral type	V	$B-V$	Reference
J083141.93+260641.0	1161-0156334	–	–	–	–	–
J083554.98+224611.3	1127-0193591	–	–	–	–	–
J083622.69+191129.3	1091-0164534	JS127	K2	12.41	1.11	2
J083627.81+175453.4	1079-0203318	JS134	F7.5	10.96	0.37	2
J083627.86+210716.2	1111-0173917	JS131	K5.9	14.04	–	2
J083628.30+201342.8	1102-0162570	KW535	K1.3	12.65	0.95	5
J083648.96+191526.4	1092-0164565	KW539	G4	10.76	–	1
J083657.82+213355.9	1115-0175522	JS156	K7.7	14.46	–	2
J083711.48+194813.2	1098-0164221	KW23	G	11.33	0.71	3
J083718.29+194156.3	1096-0163761	KW27	G5	11.45	0.74	3
J083722.23+201037.0	1101-0161763	KW30	G	11.4	0.72	3
J083727.54+193703.1	1096-0163804	KW32	G8	11.65	0.77	3
J083733.07+183915.5	1086-0168273	JS189	G0	10.6	0.74	2
J083735.77+205927.5	1109-0174003	JS190	K3.5	12.83	1.11	2
J083746.41+193557.5	1095-0163684	KW48	G8.7	12.32	0.9	4
J083747.39+190624.8	1091-0164888	KW52	G8.6	12.28	0.91	4
J084036.23+213342.1	1115-0176177	JS369	G6.2	11.64	–	2
J084245.96+211616.3	1112-0175801	–	K7.5	–	–	–
J084344.72+211234.5	1112-0175989	JS545	M0.8	15.19	–	2
J084624.31+170235.1	1070-0184311	–	–	–	–	–
J084714.12+162347.3	1063-0162881	–	F5.7	–	–	–
J084847.83+274136.5	1176-0212100	–	–	–	–	–
J083857.23+201053.6	1101-0162189	KW560	K6	13.93	1.33	4
J083902.28+191934.4	1093-0163918	KW141	K	12.39	0.93	4
J083921.54+204529.4	1107-0171494	JS286	G7.6	11.86	0	2
J083930.44+200408.6	1100-0163760	KW182	F8	10.31	0.68	3
J083935.53+185236.8	1088-0166993	KW196	G	10.73	0.65	3
J083945.78+192201.1	1093-0164074	KW208	G0	10.66	0.58	3
J084005.72+190130.7	1090-0167104	KW256	K3.2	12.62	1	4
J084022.41+203827.1	1106-0171109	JS353	K7	14.61	–	2
J084025.56+192832.8	1094-0163661	KW293	F4.8	9.85	0.47	3
J084033.46+193801.0	1096-0164636	KW313	K0.8	12.18	0.87	4
J084044.25+202818.7	1104-0163841	JS379	K6	13.93	–	2
J084047.61+185411.9	1089-0167723	KW336	G6.8	11.45	0.74	3
J084048.34+195518.9	1099-0165066	KW335	G3	11.03	0.65	3
J084055.31+183459.0	1085-0167929	JS398	K7.4	14.3	–	2
J084059.70+182204.5	1083-0186951	JS402	K2.2	11.91	1.1	2
J084122.57+185602.0	1089-0167811	KW390	K3	12.96	1.04	4
J084130.69+185218.6	1088-0167362	KW401	K3.1	12.97	1	5
J084143.67+195743.8	1099-0165295	KW417	K1.1	12.35	0.88	4
J084158.83+200627.2	1101-0162974	JS466	K4	13.23	1.11	5
J084220.09+190905.7	1091-0165816	JS482	K5	13.51	1.24	2
J084237.01+200832.0	1101-0163099	JS493	K6	13.99	1.27	5
J084248.47+203424.5	1105-0167705	JS503	K0.8	12.57	0.78	2
J084308.22+194247.7	1097-0164856	JS520	K4	13.33	1.15	5
J084317.83+203037.3	1105-0167843	JS529	K1.0	11.82	0.83	6
J084332.39+194437.8	1097-0164949	KW514	K0	12.34	0.93	4
J084519.17+190010.9	1090-0168262	JS591	K5.4	13.82	0.78	2
J084647.32+193840.9	1096-0165969	JS638	G8	10.75	0.6	6
J084817.25+165447.7	1069-0177337	–	–	–	–	–
J084948.35+160750.7	1061-0165009	–	–	–	–	–
J090222.37+182223.9	1083-0190841	–	–	–	–	–

References: 1 – Klein Wassink (1927); 2 – Jones & Stauffer (1991); 3 – Johnson (1952); 4 – Upgren et al. (1979); 5 – Weis (1981); 6 – Mermilliod et al. (1990).

This paper has been typeset from a TEX/LATEX file prepared by the author.